Załącznik nr 3

Autopresentation of scientific accomplishments (autoreferat)

1 Name

Tolga Altinoluk

2 Scientific degrees

- *May 2011* - PhD in Physics, University of Connecticut, CT, USA.
  Thesis: "*High Energy Evolution: from JIMWLK/KLWMIJ to QCD Reggeon Field Theory*"
- *March 2008* - MSc in Physics, University of Connecticut, CT, USA.

3 Employment in academic institutions

- Assistant Professor, National Centre for Nuclear Research, Warsaw (Poland).
  February 2017 - Present
- Postdoctoral Fellow, CENTRA, Instituto Superior Técnico, Universidade de Lisboa (Portugal)
  January 2016 - February 2017
- Postdoctoral Researcher, Universidade de Santiago de Compostela (Spain)
  November 2012 - January 2016
- Postdoctoral Researcher, CPHT, Ecole Polytechnique (France)
  September 2011 - November 2012
- Graduate Researcher, University of Connecticut (USA)
  May 2011 - September 2011

4 Scientific accomplishment

In the sense of article 16, paragraph 2 of the Act on Academic Degrees and Academic Title, and on Degrees and Title in Arts, 14 March 2003 (Dz. U. No 65, item 595 as amended).

a) Title of scientific achievement - a monographic series of publications

Particle production and correlations in the Color Glass Condensate

b) The monographic series of publications (authors, title, journal)

[H1] T. Altinoluk, N. Armesto, G. Beuf, M. Martinez, C. A. Salgado,
Next-to-eikonal corrections in the CGC: gluon production and spin asymmetries in pA collisions,
JHEP **1407**, 068 (2014) [arXiv:1404.2219 [hep-ph]].

[H2] T. Altinoluk, N. Armesto, G. Beuf, A. Kovner, M. Lublinsky,
Single-inclusive particle production in proton-nucleus collisions at next-to-leading order in the hybrid formalism,
Phys. Rev. D **91**, no. 9, 094016 (2015) [arXiv:1411.2869 [hep-ph]].

[H3] T. Altinoluk, N. Armesto, G. Beuf, A. Kovner, M. Lublinsky,
Bose enhancement and the ridge,
Phys. Lett. B **751**, 448 (2015) [arXiv:1503.07126 [hep-ph]].

[H4] T. Altinoluk, N. Armesto, G. Beuf, A. Moscoso,
Next-to-next-to-eikonal corrections in the CGC,
JHEP **1601**, 114 (2016) [arXiv:1505.01400 [hep-ph]].

[H5] T. Altinoluk, N. Armesto, G. Beuf, A. Kovner, M. Lublinsky,
Hanbury-Brown-Twiss measurements at large rapidity separations, or can we measure the proton radius in p-A collisions?,
Phys. Lett. B **752**, 113 (2016) [arXiv:1509.03223 [hep-ph]].

[H6] T. Altinoluk, A. Dumitru,
Particle production in high-energy collisions beyond the shockwave limit,
Phys. Rev. D **94**, no. 7, 074032 (2016) [arXiv:1512.00279 [hep-ph]].

[H7] T. Altinoluk, N. Armesto, G. Beuf, A. Kovner, M. Lublinsky,
Quark correlations in the Color Glass Condensate: Pauli blocking and the ridge,
Phys. Rev. D **95**, no. 3, 034025 (2017) [arXiv:1610.03020 [hep-ph]].

[H8] T. Altinoluk, N. Armesto, A. Kovner, M. Lublinsky, E. Petreska,
Soft photon and two hard jets forward production in proton-nucleus collisions,
JHEP **1804**, 063 (2018) [arXiv:1802.01398 [hep-ph]].

[H9] T. Altinoluk, N. Armesto, A. Kovner, M. Lublinsky,
Double and triple inclusive gluon production at mid rapidity: quantum interference in p-A scattering,
Eur. Phys. J. C **78**, no. 9, 702 (2018) [arXiv:1805.07739 [hep-ph]].

c) Description of the scientific goals and results of the series of publications with a discussion of possible applications

4.1 Introduction

High-energy hadronic collisions and heavy ions have been one of the most appealing but also challenging problems in physics for many years. They have been at the focus of theoretical effort before the proposal of Quantum Chromodynamics (QCD) as the quantum field theory to describe the strong interactions. The experimental studies to investigate QCD under extreme conditions via heavy ion collisions (HIC) started decades ago at the Brookhaven National Laboratory (BNL) and at CERN. Data from the Relativistic Heavy Ion Collider (RHIC) at BNL with nucleon-nucleon collision energies 7-200 GeV since year 2000 and, since 2010, from the heavy-ion program at the Large Hadron Collider (LHC) at CERN with collisions energies of 2.7-5.1 TeV/nucleon in PbPb and pPb runs have provided the possibility of studying a new phase of matter, called Quark-Gluon Plasma (QGP), that is described in terms of the elementary QCD quanta, quarks and gluons.

The description of the high energy collision data in proton-proton (pp) and proton-nucleus (pA) collisions are provided within the framework of an effective theory called Color Glass Condensate (CGC) that takes into account the gluon saturation effects. In this description of my scientific achievements, I provide a brief summary of my contributions that have served to the advancement of the CGC.

This report is organized as follows. In Section 4.2, I give an introduction to the concept of gluon saturation and to the CGC. In section 4.3, I concentrate on particle production in pA collisions within the CGC framework and describe the problems related with this observable and provide a description of my contributions to overcome these problems (summary of [H1], [H2], [H4], [H6] and [H8]). Section 4.4 is devoted to the description of particle correlations in this framework. In this section, I summarize my contributions to improve our understanding of the particle correlations in the CGC framework (summary of [H3], [H5], [H7] and [H9]). Finally, in Section 4.5, I describe the impact and further development of my program of studies.

4.2 The concept of gluon saturation and the Color Glass Condensate

The concept of gluon saturation was introduced via high energy evolution of the hadronic cross sections. The present section provides a review of the progress of the high energy scattering problem over the years that lead to the concept of gluon saturation to describe the high energy behavior hadronic cross sections and other relevant observables.

The problem of calculating high energy evolution of hadronic cross sections and other physical observables has a long history. It started with the early work of Gribov on reggeon field theory [1] which was performed even before the theory of strong interactions, Quantum chromodynamics (QCD), was established. High energy scattering in the framework of QCD can be studied in two different regimes. In the infrared regime, the interaction between the projectile and the target is described by "soft" scattering in which the momentum exchange between the projectile and the target is small and the theory is strongly coupled. Hence, in the soft scattering limit QCD is non-perturbative. On the other hand, one can consider the regime where the interaction between the projectile and the target is described by a "hard" scattering. In this case, the momentum transfer between the projectile and the target is large during the scattering process. Since QCD is asymptotically free, the coupling gets weaker and weaker as the momentum exchange increases. In consequence, the perturbation theory becomes more and more accurate when the relevant scale grows.

Deep inelastic scattering (DIS) with large momentum exchange is a well known process for which perturbation theory is successfully applied within the framework of QCD. In this process, Fig. 1, a virtual photon emitted by an electron scatters off a hadron. Within the Parton model, this process can be explained in a very simple manner.

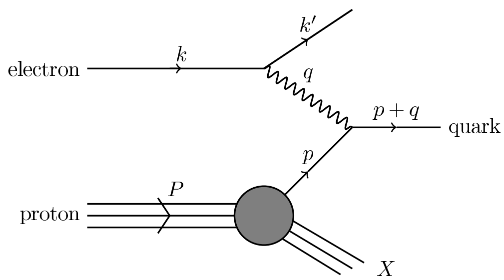

Figure 1: Deep inelastic scattering in QCD.

An incoming electron emits a virtual photon with four momenta q_μ, where the virtuality of the photon is given by $q^2 = -Q^2$, that scatters of a proton with for momenta P_μ. In this process, there are three Lorentz invariant quantities albeit only two of the are independent. The first Lorentz invariant quantity is the virtuality of the photon which is equal to the four momenta squared exchanged between the electron and the proton. The second Lorentz invariant quantity is the longitudinal momentum fraction carried by a parton inside the hadron, $x = Q^2/2P \cdot Q$. The last Lorentz invariant quantity in this process is the energy of the colliding $\gamma - p$ system which can be defined as $s \simeq 2P \cdot Q$. However, as mentioned earlier, the energy of the colliding $\gamma - p$ system is not independent and can be written in terms of the other two Lorentz invariant quantities as

$$s = \frac{Q^2}{x} \; . \tag{1}$$

The physical picture of this process within the Parton model can be described as follows. In the infinite momentum frame, the photon is a very small probe with transverse size roughly $1/Q$. In order to scatter off a proton, the photon has to encounter another object which should be roughly the same size as itself. Since quarks are charged and they interact with the photon, this object that photon has to encounter has to be a quark with the size of $1/Q$. Thus, one can think of Q as a transverse resolution scale.

One can increase the energy of the colliding $\gamma - p$ system, Eq.(1), in two ways. The first one is called "Bjorken limit" and it corresponds to the increasing the value of Q^2 for fixed value of x. In accordance with the physical picture described in the above paragraph, in the Bojrken limit increasing the energy of the colliding $\gamma - p$ system corresponds to increasing the resolution scale and decreasing the size of the probe. At the new scale, the number of partons increases simply because with a higher resolution scale one can distinguish two small transverse size partons located close to each other on the transverse plane from a single larger transverse size parton. However, the size of the resolved partons decreases much faster than the increase in their number. As a result, the density of the partons in the transverse plane decreases and the system becomes more dilute than the one we started with. This evolution associated with increasing Q^2 is described by the QCD Dokshitzer-Gribov-Lipatov-Alteralli-Parisi (DGLAP) equations [2, 3, 4]. These evolution equations describe the change of the Parton Distribution Functions (PDFs), $f_i(x, Q^2)$, with increasing Q^2 where the PDF formally can be defined as the number density of partons of type i in the proton seen with the transverse resolution scale $1/Q^2$ and carrying the longitudinal momentum fraction x.

The second way to increase the energy of the colliding $\gamma - p$ system is to consider the so called "Regge-Gribov limit". This limit corresponds to decreasing the value of x while keeping Q^2 constant to increase the energy. The first approach to describe the hadronic structure at low x is the famous Balitsky-Fadin-Kuraev-Lipatov (BFKL) equation [5, 6]. It is the perturbative linear evolution equation for the unintegrated gluon density $\phi(Y, k)$ with increasing rapidity $Y = \ln(1/x)$ that corresponds to decreasing x. The unintegrated gluon density and the gluon distribution function (gluon PDF) $f_g(x, Q^2)$ are related via

$$x f_g(x, Q^2) = \int_0^{Q^2} \frac{d^2k}{k^2}\, \phi(x, k)\ . \tag{2}$$

The BFKL evolution equation was a very important to step in the study of high energy scattering processes. It has given a lot of insight into both theoretical and experimental studies. However, it has been realized that at very high energies (or equivalently at very small values of x) BFKL equation has two major problems. The first problem is that it violates the Froissart bound [7]. In any massive theory the total scattering cross section can not grow faster than the Froissart bound $\sigma^{\rm total} < \frac{\pi}{m^2} Y^2$. However, the cross section calculated by the solution of the BFKL equation grows exponentially with rapidity, $\sigma^{\rm total} \sim e^{cY}$, hence violates the Froissart bound. Since the emitted gluons in perturbative QCD are massless, the number of gluons increases rapidly. This increases the transverse size of the hadron exponentially which leads to the violation of Froissart bound. To solve this problem one needs the information from the infrared scale of QCD. The second major problem that BFKL equation suffers from is related with the unitarity of the scattering probability. In BFKL evolution scattering probability grows without a bound and exceeds unity at rapidities of order $Y \sim \frac{1}{\alpha_s} \ln(1/\alpha_s)$. However, this problem can be addressed by taking into account the *saturation* effects.

The physical picture behind the saturation phenomena can be described as follows. In the "Regge-Gribov limit", the increase in the energy of the colliding system is achived by decreasing x while keeping Q^2 constant. This evolution causes a growth in the number of partons as well. However, this growth in the number of partons are due to parton splitting since the resolution scale is kept constant as opposed to the case in the "Bjorken limit". The parton splitting is in the longitudinal direction and the transverse scale does not change. Hence, the splitted partons have the same transverse size as the mother partons. Naturally, this increases the density of partons in the transverse plane and eventually causes saturation.

The increase in the density of partons with increasing energy has been observed in DIS. Fig.2

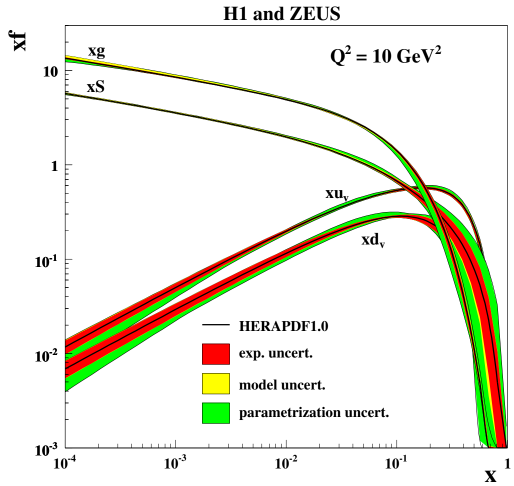

Figure 2: Parton distributions in proton (Figure taken from [8]).

is from HERA [8] and shows the rapid increase of the gluon distribution function $xf_g(x, Q^2)$ as function of x for fixed $Q^2 = 10\,\mathrm{GeV}^2$. For the values of x below 10^{-2}, the rapid rise in the number of gluons compared to quarks makes the gluons the major component of the hadronic wave function. In other words, at very high energies the effects of quarks can be neglected and gluons alone dominate partonic density of a hadron.

In DIS process, electron is used as the probe. The main reason for that is quarks carry electromagnetic charge and they interact with electron. But as explained above, in the saturation regime the main components in the hadron are gluons and quarks are neglected. Since gluons carry only color charge but not electromagnetic charge, using electron as a probe does not work. Therefore, instead of DIS, one should consider hadron-hadron scattering for studying saturation effects.

The idea of using the gluon saturation to restore the unitarity in hadron-hadron scattering was developed by Gribov, Levin and Ryskin [9]. The idea was including the nonlinear effects due to large density of gluons in the hadronic wave function. These nonlinear effects should slow down the evolution of physical observables at high energies. The GLR equation that describes the change in the gluon distribution function with decreasing x and increasing Q^2 reads

$$\frac{\partial^2\, xf_g(x, Q^2)}{\partial\, \log(1/x)\partial \log(Q^2)} = \frac{\alpha_s N_c}{\pi}\, xf_g(x, Q^2) - \frac{\alpha_s^2}{\pi^2 R^2}\, \frac{\left[xf_g(x, Q^2)\right]^2}{Q^2} \tag{3}$$

where R is the radius of the hadron. The linear term in GLR equation behaves similar to the BFKL equation and it causes a rapid growth in the number of gluons with decreasing x. During the x evolution, the nonlinear term and the linear term become comparable at some value of x. The nonlinear term stops the increase in the number of gluons and this causes *saturation*. The saturation phenomena is described by the saturation scale $Q_s(x)$ which can be interpreted as a measure of the strength of the gluon interaction processes that may occur when the gluon density becomes large.

The saturation scale can be defined in terms of the gluon distribution function as

$$Q_s^2(x) \sim x f_g(x, Q_s^2)\, \frac{\alpha_s}{\pi R^2} \tag{4}$$

Fig. 3 shows a demonstration of the phase diagram for x evolution of a hadron for different transverse momentum scale Q^2. Above the saturation line $Q_s(x)$, there is no rapid increase in the number of gluons, i.e. after saturation occurs the number of gluons in a hadron is roughly constant.

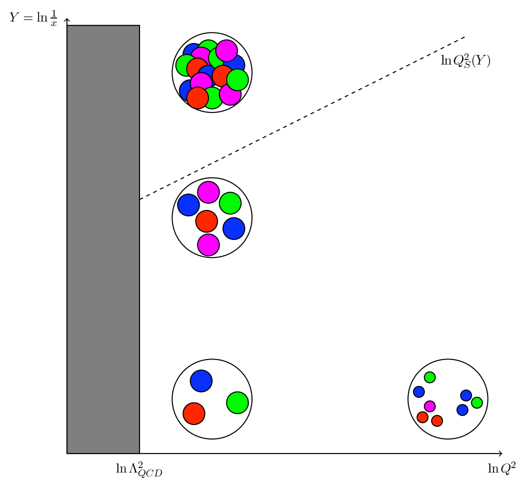

Figure 3: The sketch of the "phase-diagram" for x evolution of a hadron.

It is necessary to emphasize that GLR equation takes into account the saturation effects and it describes the evolution of the gluon distribution function both for decreasing x and increasing Q^2. However, it is more interesting to find the an evolution equation for decreasing x at fixed Q^2, in some sense the generalization of the BFKL equation, in order to probe the effects of saturation.

By introducing the color dipole model, Mueller developed gluon saturation ideas further [10, 11, 12, 13]. In this model, an incoming dipole is boosted to higher rapidity and it emits gluons as its energy increases. In the large N_c limit, a gluon line can be described by a quark- antiquark pair. Then, as the original dipole evolves, it emits another dipole at each step of the evolution. This process forms a dipole cascade and in the end the evolved system of dipoles interacts with the target. With the color dipole model, Mueller related saturation ideas to BFKL Pomeron and triple Pomeron vertex.

It was noted by McLerran and Venugopalan that a well-suited approach to the gluon saturation is to study nonlinearities of the classical Yang-Mills field theory directly in the path integral approach [14, 15]. This observation lead to what is now known as McLerran-Venugopalan model (MV model). The MV model provides the prescription of scattering processes in the saturation regime via appropriate effective degrees of freedom. These effective degrees of freedom are defined with respect to a cutoff Λ^+ imposed on the longitudinal momentum of the partons. The partons that have longitudinal momentum larger than the cutoff Λ^+ are defined by a color charge $J_a^\mu(x)$, which is the first effective degree of freedom and has the following form,

$$J_a^\mu(x) = \delta^{\mu +}\delta(x^-)\rho_a(\mathbf{x}) \; , \tag{5}$$

where $\rho_a(\mathbf{x})$ is defined as the color charge density per unit transverse area [1]. The slow gluons with longitudinal momentum smaller than the cutoff Λ^+ are defined by color field $A_a^\mu(x)$ which is the second degree of freedom in the MV model. The coupling between the slow and the fast degrees of freedom is eikonal and it is given by

$$\int d^4x J_a^\mu(x) A_{\mu a}(x) \tag{6}$$

in the action of this model. Within the MV model, the expectation value of an observable $\mathcal{O}$, that is a functional of color charge density ρ_a, is defined as

$$\langle \mathcal{O} \rangle = \int \big[D\rho_a\big]\, W[\rho_a]\, \mathcal{O}\big[\rho_a\big] \; , \tag{7}$$

where $W\big[\rho_a\big]$, which serves as a weight functional, is the distribution function of the color charge density ρ_a The reasoning behind this definition is quite simple. The color charge density ρ_a describes the distribution of the partons with longitudinal momentum larger than the cutoff Λ^+. However, this distribution ρ_a is not static and varies with time. At the time of the collision, the color charge density ρ_a describes the distribution for that specific time and one needs to average over the possible distributions $W\big[\rho_a\big]$. Thus, MV model suggests the following prescription for the computation of the expectation value of any observable: first, calculate the observable for an arbitrary configuration of the color charge densities. In the saturation regime, the nonlinearities in the color charge density ρ_a can be accounted for by solving the classical Yang-Mills equations

$$\big[D_\mu, F^{\mu\nu}\big] = J^\nu \tag{8}$$

Then as the second step, the expectation value of the observable is computed by averaging over all possible configurations via Eq. (7).

MV model successfully describes the processes like DIS at tree level. However, at any loop order it was shown that this model leads to logarithms of the cutoff Λ^+ [16]. This problem is solved by realizing that the logarithms of the cutoff Λ^+ can be absorbed into the distribution function $W\big[\rho_a\big]$ of the color charge density ρ_a which amounts to

$$W\big[\rho_a\big] \to W_{\Lambda^+}\big[\rho_a\big] \, . \tag{9}$$

Soon after this realization, the evolution equation for this cutoff dependent distribution function has been derived [17, 18, 19, 20, 21, 23, 24]. The derivation is performed by changing the cutoff Λ^+ which is imposed on the longitudinal momentum with a rapidity interval ΔY whose relation can be written as $\Delta Y = \ln\big(\Lambda_0^+/\Lambda^+\big)$. This can be interpreted as follows. At some initial rapidity Y_0, one starts with an initial distribution function $W_{\Lambda_0^+}$. As the initial rapidity changes $Y_0 \to Y$,

[1] Hereafter, boldface letters will be used for transverse components of the coordinates and momenta.

the distribution function changes from $W_{\Lambda_0^+} \to W_{\Lambda^+}$. This rapidity evolution of the distribution function is written as

$$\frac{\partial W_Y[\rho_a]}{\partial Y} = -\mathcal{H}_{\mathrm{JIMWLK}}\, W_Y[\rho_a] \tag{10}$$

This equation is known as the Jalilian-Marian-Iancu-Weigert-Leonidov-Kovner (JIMWLK) evolution equation and it is the generalization of the linear BFKL equation. $\mathcal{H}_{\mathrm{JIMWLK}}$ in Eq. (10) is the JIMWLK Hamiltonian. Here, we are not presenting the explicit expression of the JIMWLK Hamiltonian since it is not necessary for our purposes. However, it is necessary to mention that the JIMWLK evolution has limitations and it can only be employed for the scattering processes where one of the colliding objects is dilute, i.e. the number of gluons inside this object is $O(g)$, and the other one is dense, the number of gluons inside this object is $O(1/g)$, with g being the small coupling constant of QCD. I will discuss the details of this limitation and recent advances in extending its validity region in Section 5.

The "*Color Glass Condensate*" is the effective theory that describes the high energy scattering processes by employing the MV model to separate the slow and the fast degrees of freedom by imposing a cutoff on the longitudinal momentum (or equivalently on the rapidity) and employing JIMWLK evolution equation to describe the evolution with respect to this cutoff. For the simple $1 \to 1$ process, this amounts to the following prescription. The fast moving dilute projectile is described by some color charge $J^\mu(x)$ that is defined in Eq. (5). The dense target on the other hand is described by the color field which can be defined as

$$A_a^\mu(x) = \delta^{\mu -} A_a^-(x^+, \mathbf{x}) \tag{11}$$

where the target color field is assumed to be picked around $x^+ = 0$ due to Lorentz contraction. The interaction between the projectile and the target is assumed to be eikonal. At a given rapidity, this amounts to the situation where each projectile parton produced by the projectile color charge scatters on the target by picking up a Wilson line which is defined as an exponential of the target field ordered in x^+ coordinate

$$U_{\mathcal{R}}(\mathbf{x}) = \mathcal{P}_+\, e^{ig\int dx^+\, T^a_{\mathcal{R}}\, A_a^-(x^+, \mathbf{x})} \tag{12}$$

at the amplitude level. Here, $T^a_{\mathcal{R}}$ is the $SU(N_c)$ generator in the representation $\mathcal{R}$ which can be fundamental representation for a quark and adjoint representation for a gluon. The dipole operator which is defined as

$$s_R(\mathbf{x}, \mathbf{y}) = \frac{1}{D_{\mathcal{R}}}\, \mathrm{tr}\Big[U_{\mathcal{R}}(\mathbf{x}) U^\dagger_{\mathcal{R}}(\mathbf{y})\Big] \tag{13}$$

appears at the level of the cross section. Here, $D_{\mathcal{R}}$ is the color dimension of the representation and trace is performed over the color indices. As explained previously, the dipole operator is calculated for a specific distribution of target fields at some given rapidity and it has to be averaged over the possible target field distributions. Therefore, it should be written as $\big\langle s_{Y_0}(\mathbf{x}, \mathbf{y})\big\rangle$ where Y_0 is the initial rapidity and $\langle \cdots \rangle$ stands for the averaging over the target field distributions which serves as an initial condition for the rapidity evolution. In order to calculate the evolution of this observable, one should calculate the rapidity evolution of the dipole operator which is given by the JIMWLK evolution equation:

$$\frac{\partial \big\langle s_Y(\mathbf{x}, \mathbf{y})\big\rangle}{\partial Y} = -\frac{\alpha_s\, N_c}{2\pi^2} \int d^2\mathbf{z}\, \frac{(\mathbf{x}-\mathbf{y})^2}{(\mathbf{x}-\mathbf{z})^2(\mathbf{y}-\mathbf{z})^2} \Big\{ \big\langle s_Y(\mathbf{x}, \mathbf{y})\big\rangle - \big\langle s_Y(\mathbf{x}, \mathbf{z}) s_Y(\mathbf{z}, \mathbf{y})\big\rangle \Big\} \tag{14}$$

The second term on the right hand side of Eq. (14), shows that JIMWLK equation in rapidity of single dipole includes a double dipole operator. The target averaging of the double dipole operator corresponds to the situation where both dipoles $s(\mathbf{x}, \mathbf{z})$ and $s(\mathbf{z}, \mathbf{y})$ simultaneously scatter on the target. If we assume that the areas of the target on which the dipoles scatter are uncorrelated, then we can factorize the target averaging of the double dipole into target averaging of the two dipoles separately:

$$\left\langle s_Y(\mathbf{x}, \mathbf{z}) s_Y(\mathbf{z}, \mathbf{y}) \right\rangle \to \left\langle s_Y(\mathbf{x}, \mathbf{z}) \right\rangle \left\langle s_Y(\mathbf{z}, \mathbf{y}) \right\rangle \tag{15}$$

This factorization assumption reduces the JIMWLK evolution equation to Balitsky-Kovchegov (BK) evolution equation [25, 26, 27, 28].

In recent years, these developments have become the basis for phenomenological studies of saturation physics applied to high-energy collision data. As mentioned earlier, this approach is valid as long as one of the colliding objects is dilute. Typical processes that can be studied within the CGC framework are DIS on a nuclear target, DIS on a high-energy proton, proton-nucleus (pA) collisions and forward particle production in proton-proton collisions. In the rest of this report of scientific accomplishments, I will describe the specific problems that has been at the focus of the CGC, especially in pA collisions, and my contributions to the global effort of pushing the frontiers of the high-energy scattering studies within the CGC framework.

4.3 Particle production in the CGC

During the last two decades, calculations using the CGC framework have been utilized to describe different aspects of RHIC and LHC data. Even though the CGC-based data description has been quite successful, theoretical improvements are mandatory to establish its precision and determine unambiguously whether saturation is exhibited by the data. Two observables used frequently to test the compatibility of saturation physics with the proton-nucleus collision data from RHIC and the LHC experiments are particle production at central and forward rapidities. The computation framework for central production is referred to as "k_t-factorization" [29] while the one for the forward production is called "hybrid factorization" [30]. Significant part of my scientific achievements is devoted to improvement of these two frameworks.

The plan for the rest of this subsection is as follows. In part 4.3.1, I will describe k_t-factorization framework and my contributions to improve the precision of this framework concentrating on single inclusive gluon production in pA collisions. This part will be the summary of the papers [H1], [H4] and [H6] listed in the monographic series of publications. Then, in part 4.3.2, I will discuss the hybrid factorization framework for particle production at forward rapidity and explain my contributions in this framework. This part will be the summary of the papers [H2] and [H8] listed in the monographic series of publications.

4.3.1 Particle production at central rapidity and non-eikonal corrections: Summary of papers [H1],[H4] and [H6]

For single inclusive gluon production at central rapidity in pA collisions, both the projectile and the target are energetic since they are boosted from their initial rapidity to the central rapidity where the collision occurs. Therefore, in this case both of the colliding objects are treated in CGC framework. This corresponds to defining the projectile by the color charge $J_a^\mu(x)$ which is given in Eq. (5). On the other hand, the target is defined by the color field $A_a^\mu(x)$ that is given in Eq. (11). Let me recall that these expressions of the color charge of the projectile and the color field of the target are defined within the eikonal approximation. In this case one can easily calculate the production cross section of a single gluon with transverse momentum $\mathbf{k}$ and rapidity η as

$$\frac{d\sigma}{d^2\mathbf{k}d\eta} = \frac{1}{\mathbf{k}^2}\int\frac{d^2\mathbf{q}}{(2\pi)^2}\phi_P(\mathbf{q})(\mathbf{k}-\mathbf{q})^2\int d^2\mathbf{x}\,d^2\mathbf{y}\,e^{-i(\mathbf{k}-\mathbf{q})\cdot(\mathbf{x}-\mathbf{y})}s_A(\mathbf{x},\mathbf{y}) \tag{16}$$

where $s_A(\mathbf{x},\mathbf{y})$ is the dipole operator in adjoint representation that it is defined in Eq. (13) and ϕ_P is the unintegrated gluon distribution of the projectile. This is known as the k_t-factorized formula for the production cross section. In the weak field limit, it can be written as the convolution of the unintegrated gluon distributions of the projectile and the target.

The use of eikonal approximation for the projectile and the target is justified by the fact that both of the colliding objects are very energetic. Even though for the dilute projectile the eikonal approximation is very reliable, the same approximation for a large target can be true only for asymptotically large energies. The eikonal approximation for the target amounts to the following three conditions:

1. $A_a^\mu(x) \simeq \delta^{\mu-}A_a^-(x)$: Neglecting the $(+)$ and transverse components of the color field of the target.

2. $A_a^\mu(x) \simeq A_a^\mu(x^+,\mathbf{x})$: Neglecting the x^- dependence in the color field of the target.

3. $A^\mu(x) \propto \delta(x^+)$: Assuming that the target field is peaked around $x^+ = 0$ due to Lorentz contraction, which is also known as the shockwave approximation.

In realistic kinematical conditions under which the experiments are performed, the energies are not asymptotic and the eikonal approximation is not always justified. For dilute projectile it is valid even for realistic kinematics whereas this is not necessarily true for large nucleus. Relaxing any of the above approximations accounts for corrections to the eikonal limit. For a large target nucleus, the dominant contribution beyond the eikonal accuracy is obtained by relaxing the third approximation and assuming that the color field of the target is defined with a finite width L^+ along the x^+ direction. This is due to the fact that finite longitudinal width of the target is proportional to the power $A^{1/3}$ of the nuclear mass number A, and therefore this correction is enhanced with respect to the other two.

In papers [H1] and [H4], I have developed a systematic method to compute the corrections to the eikonal approximation in the CGC. Such non-eikonal corrections are originating from the finite longitudinal width of the target and can be understood as the subleading effects with respect to infinite Lorentz contraction of the target.

Before discussing the results, let me give a brief sketch of the method employed to derive the non-eikonal corrections. Let us consider the production of a single gluon with transverse momenta $\mathbf{k}$ and longitudinal momenta k^+ in pA collisions at central rapidity. The dilute projectile is still treated in eikonal approximation and it is defined with the charge density $J_a^\mu(x)$ given in Eq. (5).

On the other hand, the eikonal approximation is relaxed for the dense target and it is defined by the color field $A^\mu_a(x)$ given in Eq. (11) but instead of assuming that it is peaked around $x^+ = 0$, the color field is defined with a finite support form 0 to L^+ in the longitudinal direction. In this case, production cross section can be written as the square of the gluon production amplitude averaged over the projectile and target distributions and integrated over the impact parameter $\mathbf{B}$:

$$2k^+ \frac{d\sigma}{dk^+ d^2\mathbf{k}} = \int d^2\mathbf{B} \sum_\lambda \Big\langle \Big\langle |\mathcal{M}^a_\lambda(\underline{k}, \mathbf{B})|^2 \Big\rangle_P \Big\rangle_T \tag{17}$$

Here, λ, a and $\underline{k} = (k^+, \mathbf{k})$[2] are the polarization, color and momentum of the produced gluon. For a target with finite longitudinal width, the gluon production amplitude $\mathcal{M}^a_\lambda(\underline{k}, \mathbf{B})$ is composed of three different contributions: gluon production before the projectile propagates through the target, gluon production while the projectile is propagating through the target and gluon production after the projectile propagated through the target. At leading order, it is possible to relate the total gluon production amplitude and the background retarded gluon propagator by using LSZ reduction formula and the perturbative expansion of the color field of the target [31]. In the light cone gauge where $A^+ = 0$, the total gluon production amplitude can be written in terms of the $(i-)$ component of the background retarded gluon propagator $G^{\mu\nu}_R(x, y)$ as

$$\mathcal{M}^a_\lambda(\underline{k}, \mathbf{B}) = \epsilon^{i*}_\lambda (2k^+) \lim_{x^+ \to 0} \int d^2\mathbf{x} \int dx^- e^{ik\cdot x} \int d^4y\, G^{i-}_R(x, y)_{ab}\, J^+_b(y) \tag{18}$$

Since the color field of the target is independent of x^-, one can introduce the one-dimensional Fourier transform of the background retarded gluon propagator and write it in terms of of the background scalar propagator $\mathcal{G}^{\mu\nu}_{k^+}(\underline{x}, \underline{y})$. Then, the (i-) component of the retarded background gluon propagator reads

$$G^{i-}_R(x, y)_{ab} \int \frac{dk^+}{2\pi} e^{-ik^+(x^- - y^-)} \frac{i}{2(k^+ + i\epsilon)^2} \partial_{\mathbf{y}^i} \mathcal{G}^{ab}_{k^+}(\underline{x}, \underline{y}) \tag{19}$$

The background scalar propagator $\mathcal{G}^{ab}_{k^+}(\underline{x}, \underline{y})$ satisfies the scalar Green's equation whose solution formally can be written as a path integral

$$\mathcal{G}^{ab}_{k^+}(\underline{x}, \underline{y}) = \theta(x^+ - y^+) \int_{\mathbf{z}(y^+)=\mathbf{y}}^{\mathbf{z}(x^+)=\mathbf{x}} \big[\mathcal{D}\mathbf{z}(z^+)\big]\, e^{\frac{ik^+}{2} \int_{y^+}^{x^+} dz^+ \dot{\mathbf{z}}^2(z^+)}\, U^{ab}\Big(x^+, y^+; \big[\mathbf{z}(z^+)\big]\Big) \tag{20}$$

with the Wilson line

$$U^{ab}\Big(x^+, y^+; \big[\mathbf{z}(z^+)\big]\Big) = \mathcal{P}_+ \exp\left\{ ig \int_{y^+}^{x^+} d\tilde{z}^+\, T^c\, A^-_c\Big(\tilde{z}^+, \mathbf{z}(z^+)\Big)\right\}^{ab} \tag{21}$$

following the Brownian trajectory $\mathbf{z}(z^+)$. In the limit of vanishing longitudinal width, $x^+ - y^+ \to 0$, the background scalar propagator $\mathcal{G}^{ab}_{k^+}(\underline{x}, \underline{y})$ reduces to the standard Wilson line introduced in Eq. (12) and one recovers the eikonal limit. Therefore, it can be safely conclude that all the non-eikonal effects that are due to the finite longitudinal width of the target are encoded in the background scalar propagator. This also means that an eikonal expansion of $\mathcal{G}^{ab}_{k^+}(\underline{x}, \underline{y})$ can be performed and the

[2]Hereafter, we use the notation underline to indicate that for coordinates $\underline{x} = (x^+, \mathbf{x})$ and for momentum $\underline{k} = (k^+\mathbf{k})$.

first term in this expansion corresponds to the eikonal limit and the higher order terms correspond to the corrections to this limit.

In order to perform an eikonal expansion of the background scalar propagator $\mathcal{G}^{ab}_{k^+}(\underline{x},\underline{y})$, one should first discretize the scalar background propagator. In the eikonal limit, $k^+/(x^+-y^+)$ is much larger than any transverse scale in the problem. In the large k^+ limit, it is natural to consider a generic path as a perturbation around the classical free path

$$\mathbf{z}_n = \mathbf{z}_n^{\rm cl} + \mathbf{u}_n \tag{22}$$

where the transverse positions at step n are on the straight line $\mathbf{z}_n^{\rm cl}$

$$\mathbf{z}_n^{\rm cl} = \mathbf{y} + \frac{n}{N}(\mathbf{x}-\mathbf{y}) \tag{23}$$

between the initial and final points, and the perturbation $\mathbf{u}_n$ satisfies the boundary conditions $\mathbf{u}_0 = \mathbf{u}_N = 0$ with N being the number of discretized steps (see Fig.4-A). Once the expansion around the free classical path is performed for fixed initial and final positions, one should perform another expansion in the limit $\mathbf{u}_n \to 0$ since at each step of the discretization the transverse distance between the classical path and the initial transverse position is small (see Fig.4-B). After performing

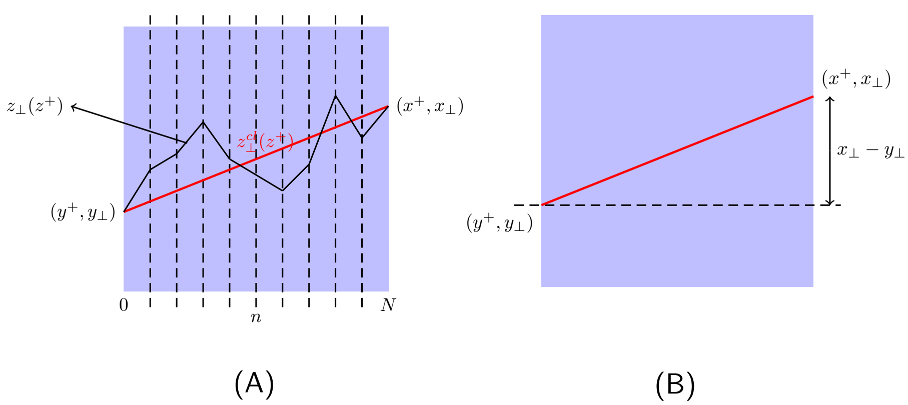

Figure 4: (A) Demonstration of the perturbative expansion around the classical path. The red line represents the classical path. At each discretization step n, the difference between the Brownian trajectory and the classical path is equal to $\mathbf{u}_n$. Perturbative expansion corresponds to Taylor expansion in the limit $\mathbf{u}_n \to 0$. (B) Demonstration of the expansion around the initial transverse position. The first expansion is performed for fixed initial and final positions. In the large k^+ limit the result has to be re-expanded since $\mathbf{z}^{\rm cl}(z^+) - \mathbf{y}$ is small at each discretization step.

these two expansions, up to second order in $(x^+ - y^+)$ - the finite longitudinal width of the target - the scalar background propagator $\mathcal{G}^{ab}_{k^+}(\underline{x},\underline{y})$ can be written as

$$
\begin{aligned}
\int d^2\mathbf{x}\, e^{-i\mathbf{k}\cdot\mathbf{x}}\, \mathcal{G}^{ab}_{k^+}(\underline{x},\underline{y}) \;=\;& \theta(x^+-y^+)e^{-i\mathbf{k}\cdot\mathbf{y}}e^{-k^-(x^+-y^+)}\Big\{U(x^+,y^+;\mathbf{y}) \\
&+\frac{(x^+-y^+)}{k^+}\Big[\mathbf{k}^iU^i_{[0,1]}(x^+,y^+;\mathbf{y})+\frac{i}{2}U_{[1,0]}(x^+,y^+;\mathbf{y})\Big] \\
&+\frac{(x^+-y^+)^2}{(k^+)^2}\Big[\mathbf{k}^i\mathbf{k}^jU^{ij}_{[0,2]}(x^+,y^+;\mathbf{y})+\frac{i}{2}\mathbf{k}^iU^i_{[1,1]}(x^+,y^+;\mathbf{y})-\frac{1}{4}U_{[2,0]}(x^+,y^+;\mathbf{y})\Big]\Big\}^{ab}
\end{aligned}
\tag{24}
$$

The first term on the right hand side of Eq.(24) is the standard Wilson line which defined in Eq. (12) that appears only at the strict eikonal order. The $O\big[(x^+-y^+)/k^+\big]$ are the first order corrections to the strict eikonal limit which we refer to as next-to-eikonal (NEik) corrections. Similarly, the $O\big[(x^+-y^+)^2/(k^+)^2\big]$ terms are the second order corrections and they are referred to as next-to-next-to-eikonal (NNEik) corrections. The terms that are denoted as $U_{[\alpha,\beta]}(x^+,y^+;\mathbf{y})$ are the *decorated* Wilson lines which only appear beyond strict eikonal order. The first subscript α in the decorated Wilson lines stands for the order of expansion around the classical path while the second subscript β stands for the order of the expansion around the initial transverse position $\mathbf{y}$. The reason why these objects are referred to as *decorated* Wilson lines is related with their structure. These objects involve a background field insertion into the standard Wilson lines along the longitudinal direction. For example the the first decorated Wilson line is defined as

$$
\Big[U^i_{[0,1]}(x^+,y^+;\mathbf{y})\Big]^{ab}=\int_{y^+}^{x^+}dz^+\frac{z^+-y^+}{x^+-y^+}U^{ac}(x^+,z^+;\mathbf{y})\big[ig\,T^e_{cd}\,A^-_e(z^+,\mathbf{y})\big]\,U^{db}(z^+,y^+;\mathbf{y})
\tag{25}
$$

The other decorated Wilson lines have similar structure with one or more background field insertions. I do not present the structure of all the decorated Wilson lines due their complexity and lengthy expressions (see [H1], [H4]). One can easily get the expression for the gluon production amplitude at NNEik accuracy given in Eq. (18) by using the expression of the retarded background gluon propagator Eq. (19) and the expression derived for background scalar propagator Eq. (24).

The retarded background gluon propagator $G^{\mu\nu}_R(x,y)_{ab}$ and therefore the scalar background propagator $\mathcal{G}^{ab}_{k^+}(\underline{x},\underline{y})$ are the main building blocks of the high energy pA collisions. In papers [H1] and [H4], the eikonal expansion performed at the level of the gluon background propagator is then applied to high energy dilute-dense scattering processes within the CGC framework. Two different observables have been analysed, in pA collisions at midrapidity, within this framework: the single inclusive gluon production cross section and the light-front helicity asymmetry of produced gluons. For the single inclusive gluon cross section, it has been shown that the NEik terms vanish and the first non-vanishing corrections to the strict eikonal limit that appear at NNEik order have been calculated. On the other hand, for the light-front helicity asymmetry, it has been shown that both the strict eikonal terms and NNEik terms vanish and the leading contribution to this observable turns out to be the NEik terms.

In [H7], I have used the results computed in [H1] and [H4] for the single inclusive gluon production cross section at NNEik accuracy and studied the weak field limit of this result. In this limit, the decorated Wilson lines are expanded to first order in the background field of the target $A^-_a(z^+,\mathbf{y})$.

For example, the decorated Wilson line $\left[U^i_{[0,1]}(x^+,y^+;\mathbf{y})\right]^{ab}$ defined in Eq. (25) reduces to

$$\left[U^i_{[0,1]}(x^+,y^+;\mathbf{y})\right]^{ab} \rightarrow \int_{y^+}^{x^+} dz^+ \, \frac{z^+-y^+}{x^+-y^+} \left[ig\, T^c_{ab}\, A^-_c(z^+,\mathbf{y})\right] \tag{26}$$

which allows us to calculate the Lipatov vertex. After expanding the eikonal and non-eikonal terms to first order in powers of the background field, the Lipatov vertex at NNEik accuracy can be written as

$$L^i_{\rm NNEik}(\mathbf{p},\mathbf{k}) = -2\bigg(\frac{\mathbf{p}^i}{\mathbf{p}^2}-\frac{\mathbf{k}^i}{\mathbf{k}^2}\bigg)\,\mathbf{k}^2\bigg\{1+\frac{i}{2}\mathbf{p}^2\frac{z_2^+}{p^+}-\frac{1}{8}\bigg(\mathbf{p}^2\frac{z_2^+}{p^+}\bigg)^2\bigg\} \tag{27}$$

Let me now, provide the interpretation of this expression with Fig. 5. The incoming projectile with transverse momenta $\mathbf{k}$ interacts with the target that has some finite longutindal extend z_2^+. The transverse momentum transfer from the target is $\mathbf{p}-\mathbf{k}$ and the produced gluon carries transverse momenta $\mathbf{p}$ and longitudinal momenta p^+.

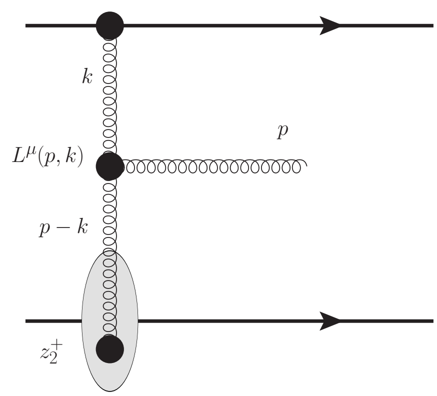

Figure 5: Illustration of the single inclusive gluon production with non-eikonal corrections to the Lipatov vertex.

The first term on the right hand side of Eq. (27) corresponds to the strict eikonal limit. The second and the third terms are the NEik and NNEik corrections respectively. The structure of the vertex suggests that the corrections to the amplitude due to finite width of the target may exponentiate [3]:

$$\bigg\{1+\frac{i}{2}\mathbf{p}^2\frac{z_2^+}{p^+}-\frac{1}{8}\bigg(\mathbf{p}^2\frac{z_2^+}{p^+}\bigg)^2\bigg\} \rightarrow \exp\bigg(i\frac{\mathbf{p}^2}{2p^+}z_2^+\bigg) \tag{28}$$

Nevertheless, let us restrict ourselves to the Lipatov vertex given at NNEik accuracy in Eq. (27). This leads to the following expression for the single inclusive gluon production cross section:

$$\frac{d\sigma}{dp^+d^2\mathbf{p}} = 4\,N_c\,(N_c^2-1)S_\perp\frac{g^2}{p^2}\left[1-\frac{1}{6}\bigg(\frac{\mathbf{p}^2\lambda^+}{2p^+}\bigg)^2\right]\int\frac{d^2\mathbf{k}}{(2\pi)^2}\phi_P(\mathbf{k}^2)\,\phi_T\big[(\mathbf{p}-\mathbf{k}^2)\big]\,. \tag{29}$$

where λ^+ is the color correlation length in the target which should be of the order of the size of a nucleon. This occurs because in the case of a finite width target, the color charge densities have

[3] This exponentiation has been proven later in Ref. [75].

the freedom to have different longitudinal positions. Thus, the correlator of such two color fields naturally introduces a dependence on the λ^+ in the observable.

$O(1)$ term in Eq.(29) is known as the k_t-factorized single inclusive cross section. The NEik terms that are $O[(\mathbf{p}^2\lambda^+)/p^+]$ drop out from the cross section as in the previous case where the cross section was written to all orders in the background field of the target. The first correction to the k_t-factorized formula appears at NNEik order. Corrections to the eikonal approximation in the k_t-factorized formula, Eq. (29), was calculated for the first time in [H7].

As already indicated above NNEik correction is suppressed by two powers of the light-cone momentum p^+ of the produced gluon but increases with transverse momentum. Nevertheless, the NNEik correction to single-inclusive gluon production is seen not to exhibit nuclear enhancement factor $A^{1/3}$ since it involves the color correlation length λ^+ rather than the target thickness L^+. However, I would like to emphasize that even with the non-eikonal corrections that are proportional to λ^+ may very well be sizable depending on the kinematics of the process. For realistic values of $\lambda^+ \simeq 0.5$ fm, relative weight of the non-eikonal corrections with respect to eikonal result can vary between %2 and %10 [75].

4.3.2 Particle production at forward rapidity: Summary of papers [H2] and [H8]

Particle production at forward rapidity in pA collisions is another observable that is used to test the compatibility of the CGC-based calculations with the data from RHIC and LHC. The state of the art calculation of this observable is based on the "hybrid formalism" [30]. In this approach, the wave function of the dilute projectile is calculated perturbatively, without any kinematic approximation, in the spirit of the collinear factorization, while the scattering of the projectile partons on the target fields is treated in the eikonal approximation within the CGC framework.

In recent years, there has been a lot of activity to calculate the single inclusive gluon production at next-to-leading order (NLO) [32, 33, 34, 35]. However, numerical studies [36] indicate very strong effects of the NLO corrections. The cross sections even become negative at moderate transverse momenta. This issue is demonstrated very clearly in Fig.6 which is taken from [36].

In [H2], I have studied the forward particle production at NLO with the aim of identifying the origin of the problem that causes the cross section to become negative and eventually solve this problem in order to stabilize the NLO corrections. The two important achievements in [H2] are: (i) to clarify the proper rapidity interval available for the evolution of the target and (ii) to correctly account for the produced pairs that are resolved by the target during the scattering.

One of the most important factors, in order to identify the origin of the negativity problem and then to correctly compute the cross section, is the choice of frame for the calculation. The most convenient frame is referred to as PROJ (projectile frame) which was introduced for the first time in [H2] since it permitted to avoid part of the problems mentioned above. In this frame, projectile moves fast enough to be able to accommodate partons with momentum fraction $x_p = p^+/P_P^+$ (longitudinal momentum fraction of the projectile carried by the produced parton). On the other

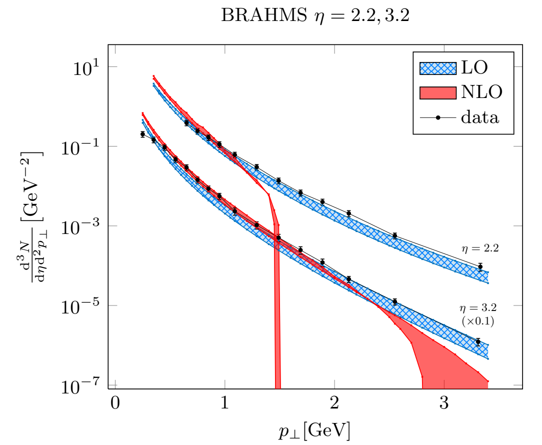

Figure 6: The data from BRHAMS collaboration [37] for charged hadron spectrum as a function of transverse momentum in dAu collisions for rapidities $\eta = 2.2$ and $\eta = 3.2$ at $\sqrt{s^{NN}} = 200\,GeV$ is plotted (figure taken from [36]). Data is compared to the numerical results calculated with rcBK gluon distribution both at LO and at NLO. Even though, the LO results fit the data fairly well, the NLO results show instability at moderate transverse momenta.

hand, target also moves fast and carries most of the energy of the process. In PROJ frame, the total energy s is defined in terms of the large momenta of the projectile $P^+_{P,\,\mathrm{PROJ}}$ and the target $P^-_{T,\,\mathrm{PROJ}}$ as

$$P^+_{P,\,\mathrm{PROJ}} = \frac{s}{2\,P^-_{T,\,\mathrm{PROJ}}} \tag{30}$$

In this frame, the large momenta of the projectile and target scale differently with energy:

$$P^+_{P,\,\mathrm{PROJ}} = \text{constant} \quad , \qquad\qquad P^-_{T,\,\mathrm{PROJ}} \propto s \tag{31}$$

We also introduce the initial energy $s_0 = 2P^+_{P,\,\mathrm{PROJ}}\,P^{-0}_T$. The final result does not depend on the initial energy explicitly. To get to the initial energy s_0, the projectile is boosted to rapidity Y_P while the target is boosted to Y^0_T from their rest frames. The distribution of the total rapidity between the projectile and the target is summarized in Fig. 7. Starting from the initial energy s_0, the energy of the process is increased by boosting the target with rapidity Y_T, such that

$$Y_T = \ln\frac{s}{s_0} \tag{32}$$

The evolution of the target from the initial rapidity Y^0_T to the final rapidity Y_T is given by the BK evolution equation that was introduced in Eq. (14) together with Eq. (15). The initial condition for the evolution of the target wave function is specified at Y^0_T. The rapidity distribution and the final rapidity evolution of the target described above is different from the standard prescription used in [33, 34, 35, 36]. The standard prescription suggests to evolve the target up to the rapidity $Y_g = \ln\frac{1}{x_g}$ where the gluon is produced. The reasoning behind this argument is that the light-cone energy, p^-, of the produced gluon is transferred from a single gluon of the target, then that gluon

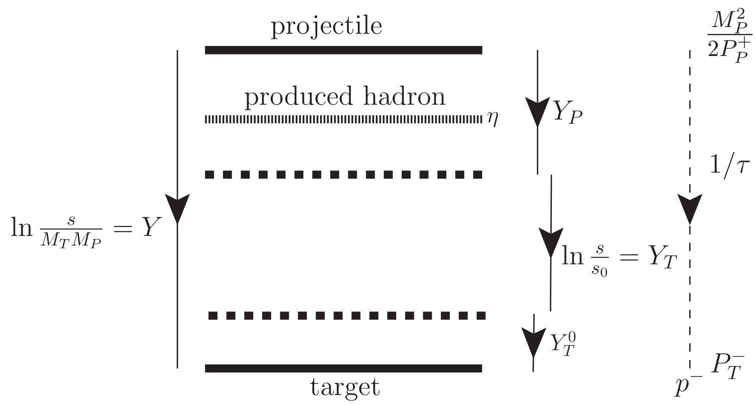

Figure 7: Illustration of the distribution of the rapidities and momentum scales in the PROJ frame.

has to carry the longitudinal momentum fraction $x_g = p^-/P^-$ of the target.

However, this argumentation over looks the fact that the target is in fact dense. The projectile parton undergoes multiple scatterings and therefore the momentum p^- it has in the final state is not transferred from a single target gluon but from several of them. This means that x_g is an upper bound on the momentum fraction of the target gluons and therefore Y_g only gives a lower bound on the rapidity up to which the target has to be evolved. Thus, it is important to use Y_T instead of Y_g for the rapidity up to which the target has to be evolved. This is the first achievement in [H2] which clearly determines the limit of the rapidity evolution of the target.

Apart from, the setting up the problem in the most convenient frame for the calculation and correctly defining the final rapidity that target is evolved, the most important new feature of the computation that I have introduced in [H2] is the so called "*Ioffe time restriction*" that provides a consistent description of the partonic configurations (pairs of partons at NLO) that are resolved by the target. This restriction can be explained as follows. In the quark channel, at LO the incoming quark scatters on the target and produces the final state particle. At NLO, the incoming quark splits into a quark-gluon pair in the projectile wave function which then scatters on the target. Within the hybrid framework, the scattering of the quark-gluon pair is treated as a completely eikonal process. This amounts to the fact that each parton gets a Wilson line during the interaction with target. However, the target has a finite longitudinal width at initial energy s_0. Therefore, this treatment is only possible if the life time of the quark-gluon pair is larger than the time that it takes to propagate thorough the target. This restriction can be formulated in the following form:

$$t_c = \frac{2\,\bar{\xi}\,\xi\,x_B P^+}{\mathbf{k}^2} > \tau \tag{33}$$

where t_c is the life time of the pair and τ is a fixed time scale determined by the longitudinal size of the target and $x_B P^+$ is the longitudinal momentum of the incoming quark, ξ is the longitudinal momentum fraction carried by the emitted gluon, $\bar{\xi} = (1-\xi)$ and $\mathbf{k}$ is the transverse momentum of the emitted gluon. This time scale τ enters into calculation via initial energy $P^+/\tau = s_0/2$. Thus, the pairs that do not live long enough are not resolved by the target. The scattering and particle production from the pairs that do not live long enough are indistinguishable from the single parent quark.

Effectively, the Ioffe time restriction appears in the calculation via replacement of the standard Weiszäcker-Williams fields $A^i(\mathbf{y}-\mathbf{z})$ by the modified one $\mathcal{A}^i_\xi(\mathbf{y}-\mathbf{z})$:

$$A^i(\mathbf{y}-\mathbf{z}) = -\frac{1}{2\pi}\frac{(\mathbf{y}-\mathbf{z})^i}{(\mathbf{y}-\mathbf{z})^2} \to \mathcal{A}^i_\xi(\mathbf{y}-\mathbf{z}) = -\frac{1}{2\pi}\frac{(\mathbf{y}-\mathbf{z})^i}{(\mathbf{y}-\mathbf{z})^2}\left[1 - J_0\left(|\mathbf{y}-\mathbf{z}|\sqrt{2\xi\bar{\xi}\frac{x_B P^+}{\tau}}\right)\right] \tag{34}$$

where J_0 is the Bessel function of the first type. When the Ioffe time restriction is discarded (in the limit $P^+/\tau \to \infty$), the modified Weiszäcker-Williams field reduces the standard one.

With the help of the two modifications described above, I calculated the quark production cross section at NLO in the hybrid formalism and showed that the NLO terms in the cross sections have two contributions

$$\left.\frac{d\sigma^{q\to H}}{d^2\mathbf{p}d\eta}\right|_{\text{NLO}} = \left.\frac{d\sigma^{q\to H}}{d^2\mathbf{p}d\eta}\right|^{\text{lit.}}_{\text{NLO}} + L_q \tag{35}$$

The first term on the right of Eq. (35) is the part of the NLO result that has been known in the literature (see for example [33, 34, 35]) and it is independent of the Ioffe time restriction. On the other hand, L_q is the new contribution that encodes the information on the Ioffe time restriction. Similarly, in the gluon channel, the new contribution L_g that accounts for the Ioffe time restriction is computed. Due to the fact these expressions are lengthy, their explicit forms are not presented here but can be found in [H2] (in Eq 3.8).

Soon after [H2] was published, the new contributions L_q and L_g are also reproduced in [38] in slightly different approach called "exact kinematical approach". The numerical studies performed in [38] show that the new contributions L_q and L_g that account for the Ioffe time restriction significantly improve the problem of negativity of the NLO cross section as can be seen from Fig. 8.

As discussed in detail in Section 4.2, within the CGC framework, the non-perturbative part of the total differential cross section that defines the structure of the hadrons is given by the parton distribution functions (PDFs) which depend on the longitudinal momentum of the parton inside the hadron. PDFs are universal objects. For certain processes, transverse momentum of the partons become important as well and these distributions need to be generalized to include the transverse momentum dependence yielding the so-called transverse-momentum-dependent distribution functions (TMDs). TMDs are process dependent unlike the PDFs and they are of great interest since their measurement offers insight on the three-dimensional structure of the hadrons.

Apart from the single inclusive particle production, hybrid formalism is also used to study forward dijet production in pA collisions [39]. This process is particularly interesting since it can be studied both in the standard TMD factorization framework (by constructing hadronic matrix elements of bilocal products of field operators that contain gauge-links) and in the CGC framework. The results obtain from two different methods should coincide when one applies the appropriate limits on both sides. Recently, it has been shown that the high energy limit of the dijet cross section calculated in the TMD factorization approach coincides with the correlation limit (when the two jets are produced back-to-back) of the cross section calculated in the CGC framework [40, 41, 42, 43].

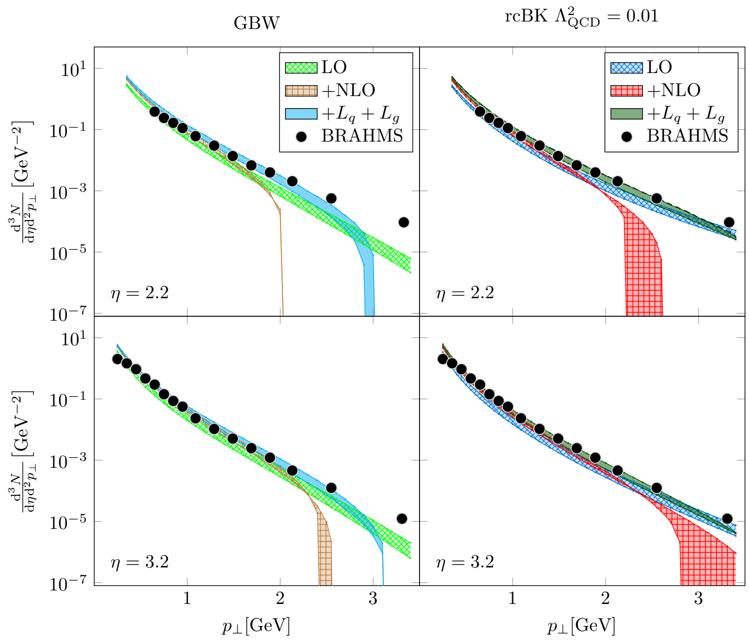

Figure 8: Figure is taken from [38]. It presents the comparison of the data from BRHAMS collaboration [37] for charged hadron spectra as a function of transverse momentum in dAu collisions for rapidities $\eta = 2.2$ and $\eta = 3.2$ at $\sqrt{s^{NN}} = 200\, GeV$ with the numerical results calculated both with GBW and rcBK gluon distribution models.

This result suggests an equivalence of the two frameworks at the appropriate limits at leading order and proves that one can get the whole set of different TMDs for these particular processes through CGC calculations.

In [H8], by using the modifications introduced in [H2] to the standard hybrid formalism, I have studied the production of three final state particles in pA collisions. Namely, the process under consideration is the forward production of a soft photon with transverse momentum $|\mathbf{q_1}| \sim Q_s$ and two hard jets with transverse momenta $|\mathbf{q_2}|, |\mathbf{q_3}| \gg Q_s$:

$$p(p_p) + A(p_A) \to \gamma(q_1) + g(q_2) + q(q_3) + X \tag{36}$$

The two important achievements in [H8] can be summarized as follows. First of all, it is the first study that provides the cross section for production of three final state particles in the hybrid formalism. Moreover, one of the produced particles is a photon and photon related observables are of key importance for the future colliders like Electron-Ion Collider (EIC) and Large Hadron electron Collider (LHeC). Second, the correlation limit of the final result provide the correspondence between the TMD and CGC frameworks beyond the simple $1 \to 2$ processes like forward dijet production.

I have adopted the same strategy to calculate the production cross section of three particles as in the case of [H2]. At order, g_e the incoming quark state is dressed by photon emission. At order g_s, it is dressed by a gluon emission. Since we are interested in the production of three final state particles, one needs to go one step further and consider the dressing of the incoming quark by a photon and a gluon at order $g_e g_s$. At this order, one should take into account two different contributions: emission of the photon before and after the emission of the gluon (see Fig. 9).

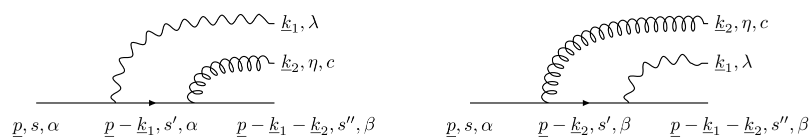

Figure 9: The dressed quark state at order $O(g_e g_s)$, with the two possible orderings of the photon resp. gluon emission by the quark.

The dressed quark state computed to order $g_e g_s$, then scatters off the target by getting a Wilson line (adjoint for a gluon and fundamental for quark) on the quark, quark-photon, quark-gluon and quark-gluon-photon components and gives the outgoing state. The relevant component of the outgoing state for the production of three particles is the quark-gluon-photon one (the other components vanish when one calculates the cross section since this is a tree level computation). Moreover, the main production mechanism of a soft photon is collinear radiation from the incoming quark which is only possible if one considers the emission of the photon before the emission of the gluon. Thus, the second ordering can be neglected. After all, this procedure provides the outgoing state and one can calculate the production cross section of a soft photon and two hard jets in straight forward manner. The final result for the cross section can be found in [H8] (Eq. 2.25). The importance of this result is that it constitutes the first step towards photon-jet production at NLO and eventually a complete NLO calculation of photon production in the hybrid formalism.

Nevertheless, the complicated final expression of the cross section can be simplified for production of jets with transverse momenta $|\mathbf{q}_2|$ and $|\mathbf{q}_3|$ much larger than the saturation momentum of the target, $|\mathbf{q}_2|, |\mathbf{q}_3| \gg Q_s$. The origin of the hard momenta of the produced jets is the large relative transverse momenta of the splitting of the quark-gluon pair in the wave function. In such a case, the transverse momentum transfer between the target and the quark-gluon pair during the scattering is small. Therefore, the final jets propagate almost back-to-back in the momentum space. The small transverse momentum imbalance of the final jets, $|\mathbf{q}_2 + \mathbf{q}_3|$, is then sensitive to the transverse momenta of the gluons in the target which are of the order of the saturations scale, i.e. $|\mathbf{q}_2 + \mathbf{q}_3| \sim Q_s$. This corresponds to a large relative momentum of the produced jets, $|\mathbf{q}_2 - \mathbf{q}_3| \gg Q_s$. Thus, in the correlation limit, we are interested in the following kinematics:

$$|\mathbf{q}_2|, |\mathbf{q}_3|, |\mathbf{q}_2 - \mathbf{q}_3| \gg |\mathbf{q}_1|, |\mathbf{q}_2 + \mathbf{q}_3| \sim Q_s \tag{37}$$

In this situation the transverse size of the produced quark-gluon pair in the coordinate space is small. This allows us to utilize a small dipole approximation and expand our final result in powers of the dipole sizes. After all said and done, the partonic cross section can be written in terms of the first two TMD gluon distributions:

$$\frac{d\sigma^{qA\to q\gamma g+X}}{d^3\underline{q}_1 d^3\underline{q}_2 d^3\underline{q}_3} \propto \alpha_s^2 \alpha_{em} \frac{1}{\mathbf{q}_1^2} \left\{ \left[\xi_2^2 - \frac{\bar{\xi}_2^2}{N_c^2} \right] \mathcal{F}_{qg}^{(1)}(x_2, P_T) + \mathcal{F}_{qg}^{(2)}(x_2, P_T) \right\} \tag{38}$$

The full expression can be found in [H8] in Eq. (3.14). Here, $P_T = \mathbf{q}_1 + \mathbf{q}_2 + \mathbf{q}_3$ and as before, $\xi_2 = q_2^+/p^+$. The functions $\mathcal{F}_{qg}^{(1)}(x_2, P_T)$ and $\mathcal{F}_{qg}^{(2)}(x_2, P_T)$ are the first two TMD gluon distributions [42] which are defined as

$$\mathcal{F}_{qg}^{(1)}(x_2, P_T) = \frac{4}{g^2}\int d^2\mathbf{b}\, d^2\mathbf{b}'\, e^{iP_T\cdot(\mathbf{b}-\mathbf{b}')} \Big\langle \mathrm{tr}\big[\big(\partial^i U_{\mathbf{b}}\big)\big(\partial^i U^\dagger_{\mathbf{b}'}\big)\big]\Big\rangle_{x_2}$$
$$\mathcal{F}_{qg}^{(2)}(x_2, P_T) = -\frac{4}{g_2}\int d^2\mathbf{b}\, d^2\mathbf{b}'\, e^{iP_T\cdot(\mathbf{b}-\mathbf{b}')} \Big\langle \mathrm{tr}\big[\big(\partial^i U_{\mathbf{b}}\big)U^\dagger_{\mathbf{b}'}\big(\partial^i U_{\mathbf{b}'}\big)U^\dagger_{\mathbf{b}}\big]\,\mathrm{tr}\big[U_{\mathbf{b}}U^\dagger_{\mathbf{b}'}\big]\Big\rangle_{x_2} \quad (39)$$

where $\langle\cdots\rangle_{x_2}$ denotes the average over the target boosted to rapidity $\ln(1/x_2)$.

The final result in the correlation limit written in terms of the TMD gluon distributions is very similar to the one for forward dijet production in the same limit [42] (up to kinematical factors due to the emission of the extra soft photon). These expressions coincide with the small-x limit of the TMD formula [39, 42] in their overlapping validity region. Obviously, the production cross section of the soft photon and two hard jets is suppressed by a power of α_{em} compared to the forward dijet production, but it is enhanced by the inverse of the transverse momentum of the soft photon in the correlation limit. Thus, the α_{em} suppression can be compensated by the transverse momenta of the soft photon which indicates that this observable might be also interesting experimentally. Moreover, Eq. (38) shows that the emission of the soft photon does not spoil the TMD structure that was seen in the forward dijet production. This shows the correspondence between the TMD and CGC frameworks beyond the simple $1 \to 2$ processes which is main achievement of [H8].

4.4 Particle correlations in the CGC: Summary of papers [H3], [H5], [H7] and [H9]

The LHC data has shown some very surprising and unexpected aspects of QCD dynamics, particularly in small systems like pp and pA. One of the most exciting observations already made during the first LHC run by the CMS collaboration in high multiplicity pp collisions, is the discovery of the correlations between produced particles over large intervals of rapidity peaking at zero relative azimuthal angle [44, 45, 46]. This was dubbed “ridge” due its shape on the azimuthal angle-rapidity plot, and constitute one of the key findings of the LHC regarding QCD dynamics (see Fig. 10). Later on, a similar ridge structure was also observed in pPb collisions at the LHC by the four large collaborations [47, 48, 49, 50]. A peak in the correlations also appears at azimuthal angle π . Similar correlations were observed earlier at RHIC in Au-Au collisions [51, 52, 53]. These collective features of particle production are surprising, since they appear in processes where the final state has the size of a single proton, which were not expected to show collective behavior similar to heavy ion collisions (HICs). Earlier observations of the ridge in HICs at RHIC have an accepted explanation as the collective flow due to strong final state interactions, usually described in the framework of relativistic viscous hydrodynamics. Such explanation in pp collisions looks tenuous for several reasons, in particular due to the small system size. Nevertheless, data can be well described by hydrodynamic simulations. This naturally raises a fundamental question: is the strong interaction dynamics capable to lead to collectivity even in small systems, or is the origin of the ridge correlations different in pp and pPb collisions than in HICs?

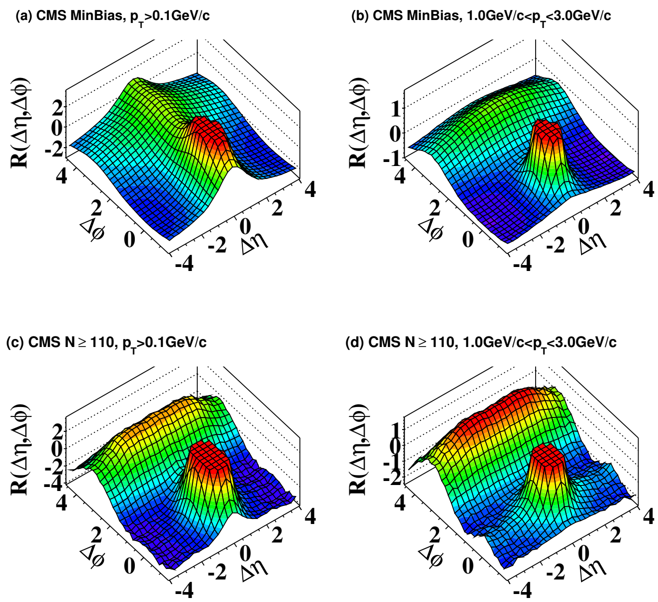

Figure 10: Figure taken from [44]. Two dimensional plot for two-particle correlation functions for 7 TeV pp collisions. (a) minimum bias events with $p_t > 0.1$ GeV/c, (b) minimum bias events with $1 < p_t < 3$ GeV/c, high multiplicity events with $p_t > 0.1$ GeV/c and (d) high multiplicity with $1 < p_t < 3$ GeV/c. The ridge structure is apparent in figure (d).

Significant part of my scientific achievements is devoted to understand whether the structure of the initial state itself can lead, in pp and pA collisions, to such correlations independently of strong final state interactions. Over the last decade, several mechanisms have been suggested to explain the ridge correlations in the CGC framework. The most successful one is the so-called the "glasma graph" approach [54, 55, 56]. Even though this approach is very successful to describe the data [57, 58, 59, 60, 61, 62], the physics behind it was not clear.

In [H3], I have studied the two particle correlations within the "glasma graph approach" and have shown that Bose enhancement of the gluons in the projectile wave function leads to final state correlations in this approach. This is the main achievement of [H3].

The concept of Bose enhancement for a generic quantum system can be understood by considering a state with fixed occupation number, $\{n_i(p)\}$, of N species of bosons at different momenta which up to some normalization function can be written as

$$\big|\{n_i(p)\}\big\rangle \propto \prod_{i,p} \big[a_i^\dagger(p)\big]^{n_i(p)}|0\rangle \tag{40}$$

with $a_i^\dagger(p)$ being the creation operator of the boson and $i = 1, 2, \ldots, N$. The mean particle density $\tilde{n}$ is defined as the expectation value of the number operator in this state:

$$\tilde{n} \equiv \big\langle\{n_i(p)\}\big|\sum_j a_j^\dagger(x)a_j(x)\big|\{n_i(p)\}\big\rangle = \sum_{i,p} n_i(p) \tag{41}$$

The two particle correlator in momentum space $D(p,k)$ is defined in a similar way and can be calculated in a trivial manner:

$$D(p,k) = \Big[\sum_i n_i(p)\Big]\Big[\sum_j n_j(k)\Big] + \delta(p-k)\sum_i \big[n_i(p)\big]^2 \tag{42}$$

The first term on the right hand side of Eq. (42) is the square of the mean particle density and the second term is the Bose enhancement term. It vanishes when the momentum of the two bosons are different and gives an enhancement which is $O(1/N)$ when the momenta of two bosons are same. The Bose enhancement term is $O(1/N)$ due to the fact that it contains a single sum over the species index. The physics behind this is the fact that only bosons of the same species are correlated with each other.

Let me now, describe how Bose enhancement arises in the CGC and lead to final state correlations by considering the double inclusive gluon production within the glasma graphs approach. In this approach each produced gluon is assumed to be produced from a different color charge denisty in the projectile wave function. For our purposes, these color charge densities can be conveniently represented in terms of gluon creation and annihilation operators in the incoming projectile wave function. After averaging over the target fields the glasma graphs can be written as sum of three types of diagrams (see Fig. 11). Type A diagram describes the case where the two gluons with

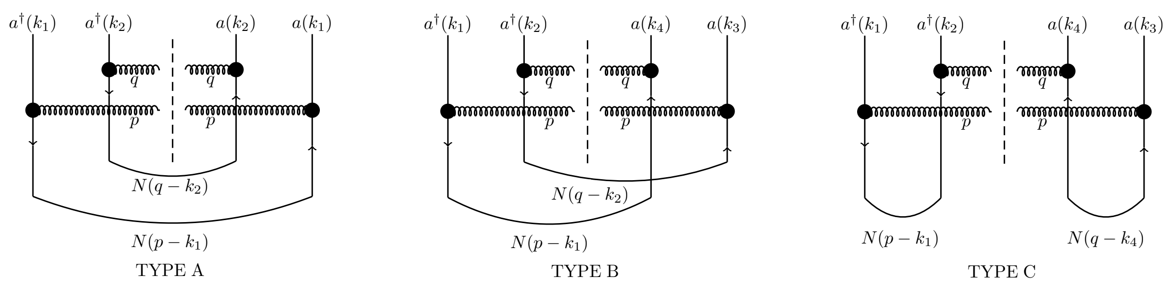

Figure 11: Glasma graphs for two gluon inclusive production before averaging over the projectile color charge density ρ. Black blobs denote vertices and dashed lines the cuts.

transverse momenta $\mathbf{k}_1$ and $\mathbf{k}_2$ scatters independently on the target by acquiring transfer of transverse momentum $\mathbf{p}-\mathbf{k}_1$ and $\mathbf{q}-\mathbf{k}_2$ so that the outgoing gluons have transverse momenta $\mathbf{p}$ and $\mathbf{q}$. Type B and Type C diagrams include interference contributions which are also interesting to study but the Bose enhancement effect can be observed by studying the Type A diagrams alone, so here I only concentrate on this diagram. The Type A contribution to the double inclusive gluon production is proportional to (see Eq.(7) in [H3] for the full expression)

$$\text{Type A} \propto \int \frac{d^2\mathbf{k}_1}{(2\pi)^2}\frac{d^2\mathbf{k}_2}{(2\pi)^2}\,\langle \text{in}|a_a^{\dagger i}(\mathbf{k}_1)a_b^{\dagger j}(\mathbf{k}_2)a_a^k(\mathbf{k}_1)a_b^l(\mathbf{k}_2)|\text{in}\rangle\, N(\mathbf{p}-\mathbf{k_1})\, N(\mathbf{q}-\mathbf{k_2}) \tag{43}$$

where $N(\mathbf{p}-\mathbf{k})$ is the dipole scattering amplitude. Moreover, the rapidity dependence on the gluon creation and annihilation operators are integrated over. The explicit dependence on rapidity becomes important when the rapidity difference between the observed particles is large, $\Delta\eta \sim 1/\alpha_s$.

The evaluation of the expectation value of any operator in the incoming projectile state requires two averaging procedure in the CGC. In [H3], I performed first averaging over the valance color charge density that leads to the density matrix operator $\hat{\rho}$, on the soft gluon Hilbert space (see Eq. (15) in H[3] for the explicit expression). Then, I have performed the second averaging over the soft gluons by using this density matrix operator. The two particle correlator that appears in Type A contribution calculated with this procedure lead to the following result (see Eq.(18) in [H3] for the explicit expression):

$$D(\mathbf{k}_1, \mathbf{k}_2) \propto \left\{ 1 + \frac{1}{S_\perp (N_c^2 - 1)} \Big[\delta^{(2)}(\mathbf{k_1} - \mathbf{k_2}) + \delta^{(2)}(\mathbf{k_1} + \mathbf{k_2}) \Big] \right\} \tag{44}$$

where $S_\perp$ is the transverse area of the projectile. The first term on the right hand side of Eq. (44) is the classical term which corresponds to the square of the number of gluons while the second term is the typical Bose enhancement term.

If we consider a situation where the incoming projectile has intrinsic saturation momentum Q_s and the momenta of the produced gluons are of the same order as Q_s, i.e. $|\mathbf{p}| \sim |\mathbf{q}| \sim Q_s$, then the production amplitude is dominated by the contributions $|\mathbf{k}_1| \sim |\mathbf{k}_2| \sim Q_s$. The initial state correlations are encoded in the Bose enhancement terms in Eq. (44) which are delta functions. The interaction with the target is obtained by convoluting the two particle correlator with the dipole amplitudes $N(\mathbf{p} - \mathbf{k_1})N(\mathbf{q} - \mathbf{k_2})$. Since in this kinematics, the momentum transfers from the target ($|\mathbf{p} - \mathbf{k_1}| \sim |\mathbf{q} - \mathbf{k_2}| \ll Q_s$) are small and since the Bose enhancement terms involve delta functions, these initial state correlations naturally transform into angular correlations between the directions of the vectors $\vec{p}$ and $\vec{q}$ in the final state. In more general cases, the delta functions are smeared when convoluted with the dipole scattering amplitudes but this does not spoil the final state angular correlations. This identification of the origins of the final state angular correlations is the main achievement in [H3].

The immediate question that arises after the study of [H3]: "are the quarks are subject to correlations in the CGC?" In [H7], I have addressed this question and study the correlations between the produced quarks for the first time in the CGC framework. The results of [H3] shows that the origin of the correlations between the produced gluons is the Bose enhancement of the projectile gluons. Due to their fermionic nature, one expects quarks to experience Pauli blocking which effectively amounts to a suppression of the probability of finding two quarks with the same quantum numbers in the CGC state. Therefore, one should expect negative correlation between the final state quarks that originate from the initial state ones. On the other hand, the correlation between the gluons is found to be long range in rapidity since the CGC wave function is dominated by the rapidity integrated soft gloun field. Thus, another important question to answer: are the (anti)correlations between the final state quarks long or short range in rapidity? The answer to this question is not obvious a priori. In the projectile wave function, quarks are produced via splitting of the rapidity invariant gluons into quark-antiquark pairs. However, the splitting amplitude itself depends on the rapidity of the quark and antiquark. Moreover, due to this splitting in the projectile wave function the expression for the production cross section of quarks is much more complicated when compared to the gluons.

The main achievements in [H7] are the answers of these two questions. In [H7], I have shown that the initial state correlations between the quarks in the projectile wave function are not distorted by small momenta transfer from the target in specific kinematics. In this kinematics the rapidity difference between the produced quarks is relatively large, i.e. $\eta_1 - \eta_2 \gg 1$. Moreover, the transverse momenta of the produced quarks $\mathbf{p}$ and $\mathbf{q}$ are of the same order and much larger than the saturation scale of the projectile Q_s, and the saturation scale of the projectile is much larger than saturation scale of the target Q_T, i.e. $|\mathbf{p}| \sim |\mathbf{q}| \gg Q_s \gg Q_T$. In this kinematics the contribution to the production cross section that is sensitive to correlations has the following form (see Eqs. (3.19) and (3.20) in [H7] for the full expressions)

$$\frac{d\sigma}{d^2\mathbf{p}d\eta_1\, d^2\mathbf{q}d\eta_2}\bigg|_{\text{corr.}} \propto -e^{-(\eta_1-\eta_2)}(\eta_1-\eta_2)^2\Big] \tag{45}$$

The negative sign of this contribution shows that it suppresses the classical term as opposed to the gluonic case. This is the result of the Pauli blocking effect in the quark-quark production. Moreover, this effect decays exponentially with the rapidity difference between two produced quarks which shows that it is short range in rapidity. However, this exponential decrease is tempered by two powers of the rapidity difference.

In [H5], I have shown that there is another physical effect present in the glasma graph approach which is referred to as the Hanbury-Brown-Twiss (HBT) correlations between the produced gluons. The diagrams in the "glasma graphs approach" that lead to the HBT correlations are presented in Fig. 12 after performing pair wise contraction of the color charges in the projectile wave function. Assuming translationally invariant projectile wave function, the contribution from the Type B and

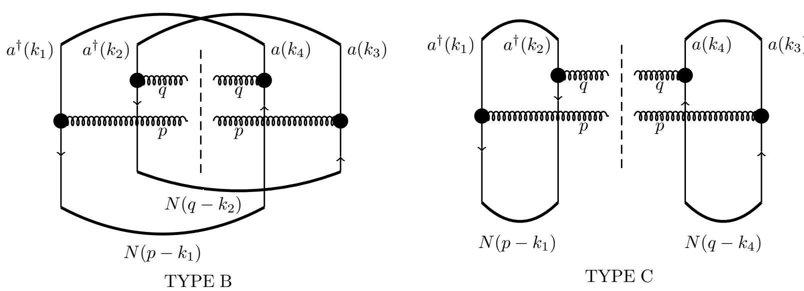

Figure 12: Glasma graph diagrams (after averaging over the projectile color charges) that lead to HBT correlations.

Type C diagrams to the production cross section is

$$\text{Type B} \propto \delta^{(2)}(\mathbf{p}-\mathbf{q})\,, \qquad \text{Type C} \propto \delta^{(2)}(\mathbf{p}+\mathbf{q}) \tag{46}$$

If the translational invariance condition is relaxed, then the delta functions are smeared over the scale of the size R of the projectile: $|\mathbf{p} \pm \mathbf{q}| \sim R^{-1}$. This size R represents the radius of the gluon cloud inside the proton and its inverse is smaller than the saturation scale, $R^{-1} < Q_s$. Moreover, I have shown in [H5] that the HBT correlations are long range in rapidity just as the Bose enhancement effect. This amounts to the fact that, the strength of the HBT correlations is equal when the rapidities of the two produced gluons are equal ($\eta_1 = \eta_2$) or when the difference between them is large ($|\eta_1 - \eta_2| \gg 1$).

These findings can be summarized as follows. The correlation function $C(\mathbf{p}, \mathbf{q})$, which is formally defined as the ratio of double inclusive gluon production cross section to the square of the single one, in the "glasma graph approach" contains two physical effects which can be written as follows:

$$C(\mathbf{p}, \mathbf{q}) = 1 + C(\mathbf{p}, \mathbf{q})\Big|_{\mathrm{BE}} + C(\mathbf{p}, \mathbf{q})\Big|_{\mathrm{HBT}} \tag{47}$$

The first term on the right hand side of Eq. (47) is the classical contribution which originates from the square of the single inclusive production. $C(\mathbf{p}, \mathbf{q})\big|_{\mathrm{BE}}$ represents the effect of Bose enhancement of the gluons in the projectile wave function. As described above, this effect leads to the correlation of the final state gluons. On the other hand, $C(\mathbf{p}, \mathbf{q})\big|_{\mathrm{HBT}}$ represents the HBT correlations in the "glasma graph approach" which directly introduces correlations between the final state gluons. Both $C(\mathbf{p}, \mathbf{q})\big|_{\mathrm{BE}}$ and $C(\mathbf{p}, \mathbf{q})\big|_{\mathrm{HBT}}$ are rapidity independent which shows that both effects are long range in rapidity. The Bose enhancement contribution is suppressed by a factor of the transverse area of the projectile with respect to HBT contribution. However, it leads to correlations whose width in the momentum space is determined by the saturation momentum Q_s. On the other hand, the HBT contribution is not suppressed but it gives a narrow peak in momentum space with the width R^{-1}. This comparison is demonstrated in Fig. 13. The main achievements in [H5] are the

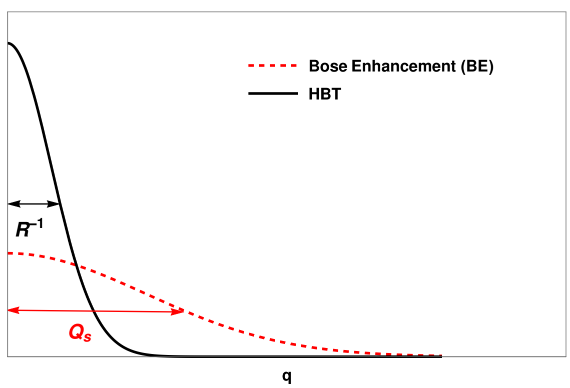

Figure 13: Schematic separation in q of the contribution to the HBT effect (solid line) and contribution to the Bose enhancement effect (dashed line) in two-particle correlation function.

identification of the HBT effect in the glasma graph approach and its comparison with the Bose enhancement effect which is summarized in Fig. 13.

The "glasma graph approach" to double inclusive particle production is valid for pp collisions. In principle, the dipole scattering amplitudes $N(\mathbf{p} - \mathbf{k_1})$ and $N(\mathbf{q} - \mathbf{k_2})$ introduced in Eq. (43) are assumed to originate from single target fields and therefore this approach does not take into account the effects of multiple scatterings in the dense target. In [H9], I have extended this study and computed the inclusive production of two and three particles beyond "glasma graph approach" by including the multiple scattering effects. Thus, the results of [H9] extends the validity of the "glasma graph approach" from pp to pA collisions which is one of the main achievements in [H9].

Apart from taking into account the multiple scattering effects in [H9], I have also introduced a systematic way to identify each term and describe whether it is a Bose enhancement or HBT contribution. For this identification, I have used the following strategy. When calculating the double inclusive gluon production, one has to average over four color charges (two in the amplitude and two in the complex conjugate amplitude) in the projectile wave function: $\langle \rho^{a_1}(\mathbf{x_1})\rho^{a_2}(\mathbf{x_2})\rho^{b_1}(\mathbf{y_1})\rho^{b_2}(\mathbf{y_2})\rangle_P$. Here, $\mathbf{x_i}$ and $\mathbf{y_i}$ stands for the transverse position of the the color charge densities in the amplitude and in the complex conjugate amplitude respectively. The averaging over the color charge distributions in the projectile is performed by using a generalized MV model where the weight functional is Gaussian. Then, the average of any product of color charge densities factorizes into a product of all possible Wick contractions. The correlator of two color charge densities in momentum space can be defined as

$$\langle \rho^a(\mathbf{k})\rho^b(\mathbf{k})\rangle_P = \delta^{ab}\mu^2(\mathbf{k},\mathbf{p}) \tag{48}$$

This function $\mu^2(\mathbf{k},\mathbf{p})$ defines the structure of the projectile and it can be written as

$$\mu^2(\mathbf{k},\mathbf{p}) = T\left(\frac{\mathbf{k}-\mathbf{p}}{2}\right)F\big[(\mathbf{k}+\mathbf{p})R\big] \tag{49}$$

where $F\big[(\mathbf{k}+\mathbf{p})R\big]$ is a soft form factor which is maximal at F(0), and R is the radius of the projectile. The function T defines the transverse momentum dependent distribution of the valence charges. The soft form factor identifies whether a term is a contribution to the Bose enhancement of the projectile gluons or a contribution to the HBT correlations of the produced gluons. For example, in our set up the produced gluons have momenta $\mathbf{p}$ and $\mathbf{q}$, while the projectile gluons carry transverse momenta $\mathbf{k_1}$ and $\mathbf{k_2}$. In this case, the $\mu^2(\mathbf{p},\mathbf{q})$ give maximal contribution when $\mathbf{p}+\mathbf{q}=0$ which clearly can be identified as the HBT correlations of the produced gluons. The $\mu^2(\mathbf{k_1},\mathbf{k_2})$ is peaked when $\mathbf{k_1}+\mathbf{k_2}=0$ which is a contribution to the Bose enhancement of the gluons in the projectile wave function.

On the other hand, the multiple scattering effects on the dense target are taken into account via adjoint Wilson lines $U^{ab}(\mathbf{x})$ in gluon production process as described in detail in Section 4.2. This leads to the appearance of double dipole and quadrupole amplitudes (in the adjoint representation) of the type

$$\langle s(\mathbf{x},\mathbf{y})s(\mathbf{z},\mathbf{w})\rangle_T \qquad \langle Q(\mathbf{x},\mathbf{y},\mathbf{z},\mathbf{w})\rangle_T \tag{50}$$

in the cross section, which have to be averaged over the target field distributions. The double operator is expressed in terms of dipole amplitude $s(\mathbf{x},\mathbf{y})$ is defined in Eq. (13) and the quadrupole amplitude is defined as

$$Q(\mathbf{x},\mathbf{y},\mathbf{z},\mathbf{w}) = \frac{1}{N_c^2-1}\mathrm{tr}\big[U(\mathbf{x})U^\dagger(\mathbf{y})U(\mathbf{z})U^\dagger(\mathbf{w})\big] \tag{51}$$

The cross section has to be integrated over four transverse coordinates. In principal, the maximal contribution should come from the area in coordinate space, i.e. when all the four coordinates are far away from each other. However, all four points can not be far away from each other since the target field ensemble has to be color nuetral. Therefore, the maximal contribution must come from the configurations where the four points are combined into pairs, such that each pair is a singlet and the distance between the pairs is large. Taking into account only such configurations is equivalent to calculating the target averages of product of any number of Wilson lines by factorizing them into averages of pairs with basic Wick contraction. In this case, the the quadrupole amplitudes can be written as

$$\langle Q(\mathbf{x},\mathbf{y},\mathbf{z},\mathbf{w})\rangle_T = \langle s(\mathbf{x},\mathbf{y})\rangle_T \langle s(\mathbf{z},\mathbf{w})\rangle_T + \langle s(\mathbf{x},\mathbf{w})\rangle_T \langle s(\mathbf{z},\mathbf{y})\rangle_T + \frac{1}{N_c^2-1}\langle s(\mathbf{x},\mathbf{z})\rangle_T \langle s(\mathbf{y},\mathbf{w})\rangle_T \quad (52)$$

Similar expression for double dipole operator can be found in [H9] in Eq (18). Then, by using the function $\mu^2(\mathbf{k},\mathbf{p})$ given in Eq.(49) for the projectile color charge density correlators and using the factorization ansatz described above for the double dipole and quadrupole amplitudes, I have calculated the double inclusive gluon production cross section and identified the nature of all the terms. Moreover, I have used same computation framework to compute the inclusive production of three gluons and identify each term whether they are contributions to the Bose enhancement of the projectile gluons or contribution to the HBT correlations of the final state gluons.

The main achievements in [H9] can be listed as follows. First of all, I introduced the function $\mu^2(\mathbf{k},\mathbf{p})$ and used the factorization argument of the averaging over the target field configurations which can be applied to production of any number of gluons in pA collisions. This procedure establishes a systematic way of identification of whether a term is a contribution to the Bose enhancement of projectile gluons or a contribution to HBT correlations of the final state particles. Second, with this approach I have computed inclusive production of both two and three gluons. I have shown that, the contributions to the final state correlations are originating from quadrupole terms in the two gluon production. Similarly, the correlations between the three final state gluons are originating from sextuple amplitude (trace of six Wilson lines) in the three gluon production process.

4.5 Impact and prospects

As described in detail in Sections 4.3 and 4.4, with the results of the works that have been presented here, I have significantly improved our understanding of saturation phenomena and the CGC framework. In particular, the non-eikonal study of the single inclusive gluon production in pp and pA collisions developed in [H1], [H4] and [H6] have triggered many studies in the CGC framework especially in the context of TMDs [63, 64] and spin related observables [65, 66, 67]. On the other hand, the idea of "Ioffe time restriction" that was introduced in [H2] in order to stabilize the NLO corrections to the single inclusive particle production in the hybrid formalism is further developed in [68], and a new factorization scheme is proposed for this process. Finally, the results of my contributions in [H3], [H5], [H7] and [H9] are used in many numerical studies for the explanation of the two particle correlations within CGC framework (see for example [69, 70, 71]).

The results of the works that I present here can inspire further studies in the CGC framework. One of the immediate direction is related with the two particle correlations. The key theoretical problem for the description of the two particle correlations within CGC is the absence of the odd harmonics in the azimuthal angle ϕ, i.e. terms containing $\cos(n\phi)$ with n being odd. This issue is recently addressed and it has been shown that inclusion of higher-order saturation corrections in the projectile wave function generates non-vanishing odd harmonics [72, 73]. It has been shown in [74], the description of the data is possible by including these density corrections. Very recently, I have also studied the problem of vanishing odd azimuthal harmonics in the CGC framework in [75]. In this work, I have shown that including the non-eikonal corrections in the study of the two particle correlations in pp collisions also leads to non-vanishing odd harmonics. Currently, I am working on a more dedicated numerical study of the odd harmonics originating form the non-eikonal corrections in pp collisions.

On the other hand, I have recently extended the study performed in [H8] and considered the forward production of two hard jets and a hard photon [76]. The main difference in the new study is that the produced photon is not restricted to be soft. This leads to the possibility of production of the final state photon in the gluon initiated channel which was absent in [H8]. In [76], I have shown that in the correlation limit of the cross section of this process one probes, in the quark channel, the first two unpolarized TMDs defined in Eq. (39) together with their linearly polarized partners. Moreover, in the gluon channel one probes the first three TMDs of this channel with their linearly polarized partners. These two studies performed in [H8] and in [76] constitute the first steps of the computation of the production of a photon and a single jet at NLO. This is another problem that I am working on currently which will show the correspondence between the CGC and TMD frameworks at NLO.

Also very recently, in [77] and [78], I have shown how the CGC formulation which involves the Wilson lines can be fully rewritten as an infinite twist TMD framework for inclusive observables. This leads to a perfect match between the high and moderate energy limits of QCD given in terms of TMDs and PDFs. The immediate continuation of these studies is its application to the azimuthal angular correlations in the DIS dijet production.

5 Other scientific achievements

5.1 Bibliometric data (as of March, 2019)

According to the Web of Science

number of citations: 245
number of citations without self-citations: 213
h-index (Hirsch index): 9
total impact factor (the sum of 5-year journal impact factors [H1]-[H9], [P1]-[P7]): 71,683

5.2 Description of other scientific achievements

5.2.1 Other publications after completing PhD studies

The list of my other publications after PhD is as follows.

[P1] T. Altinoluk, B. Pire, L. Szymanowski, S. Wallon, *Resumming soft and collinear contributions in deeply virtual Compton scattering*, JHEP **1210**, 049 (2012) [arXiv:1207.4609 [hep-ph]].

[P2] T. Altinoluk, C. Contreras, A. Kovner, E. Levin, M. Lublinsky, A. Shulkin, *QCD Reggeon Calculus From KLWMIJ/JIMWLK Evolution: Vertices, Reggeization and All*, JHEP **1309**, 115 (2013) [arXiv:1306.2794 [hep-ph]].

[P3] T. Altinoluk, A. Kovner, E. Levin, M. Lublinsky,
Reggeon Field Theory for Large Pomeron Loops,
JHEP **1404**, 075 (2014) [arXiv:1401.7431 [hep-ph]].

[P4] T. Altinoluk, N. Armesto, A. Kovner, E. Levin, M. Lublinsky,
KLWMIJ Reggeon field theory beyond the large N_c limit,
JHEP **1408**, 007 (2014) [arXiv:1402.5936 [hep-ph]].

[P5] T. Altinoluk, N. Armesto, G. Beuf, A. H. Rezaeian,
Diffractive Dijet Production in Deep Inelastic Scattering and Photon-Hadron Collisions in the Color Glass Condensate,
Phys. Lett. B **758**, 373 (2016) [arXiv:1511.07452 [hep-ph]].

[P6] T. Altinoluk, N. Armesto, G. Beuf, A. Kovner, M. Lublinsky,
Heavy quarks in proton-nucleus collisions - the hybrid formalism,
Phys. Rev. D **93**, no. 5, 054049 (2016) [arXiv:1511.09415 [hep-ph]].

[P7] T. Altinoluk, N. Armesto, D. E. Wertepny,
Correlations and the ridge in the Color Glass Condensate beyond the glasma graph approximation,
JHEP **1805**, 207 (2018) [arXiv:1804.02910 [hep-ph]].

Now, I would like to describe shortly each of the work performed in the publications listed above.

The JIMWLK equation takes into account the nonlinear effects of the large gluon density of the projectile evolution. However, at very high energies where one can evolve in energy both colliding objects, there is another nonlinear effect that comes into play, namely multiple scatterings on a dense target. Such scattering processes are outside of the validity of JIMWLK equation. This makes it inapplicable for processes with a very large range of evolution in rapidity, which evolve an initially dilute projectile into a dense system at final energy. During my PhD studies, I have worked on the derivation of a new Hamiltonian which leads to generalization of the JIMWLK equation that takes into account both of the above mentioned effects via Pomeron loops [79, 80]. This Hamiltonian of QCD is referred to as "Reggeon Field Theory (RFT) Hamiltonian of QCD" since it clarifies the relation between the functional evolution approach and the QCD formulation of pre-QCD ideas known as reggeon field theory. After my PhD apart from the new topics that I have worked on, I also continued on this direction of research. In [P2], I have extended the study of the RFT Hamiltonian of QCD by considering the rapidity evolution in terms of the natural degrees of freedom of this theory which are refered to as the reggeons. In [P3], I have analyzed the range of applicability of this state-of-the-art Hamiltonian. I have shown that this approach partially overcomes the limitations of BK-JIMWLK formulation. However, the new Hamiltonian is only as long as at any intermediate value of the rapidity throughout the evolution at least one of the colliding objects is dilute. Finally, in [P4], I have studied the relation between the RFT Hamiltonian and the functional JIMWLK equation beyond the simplified large N_c limit.

After my PhD, I got interested in the study of the exclusive physics and the Generalized Parton Distributions (GPDs) that are nonperturbative objects and can be considered as the generalization of the TMDs. In [P1], I have focused on Deeply Virtual Compton Scattering (DVCS), particularly to the quark channel. The quark coefficient function which can be calculated perturbatively includes double logarithmic terms of the light cone momentum fraction of the incoming and outgoing quarks at NLO. These terms become important in the limit of vanishing light cone momentum fraction. I have performed an all order resummation of these double logarithmic terms and provided a simple resummed expression for the quark coefficient function.

In [P5], I have studied the diffractive dijet production in DIS and in photon-hadron collisions within the CGC framework. The results showed that the diffractive dijet cross section shows sensitivity to the orientation of the dipole in the transverse plane. In other words, the cross section depends both on the dipole transverse size $\mathbf{r}$ and its impact parameter $\mathbf{b}$. This result suggests that this observable can be used to study the possible correlations between the produced quark-antiquark pair such as the azimuthal angle correlations.

[P6] is a natural continuation of the study performed in [H2]. In this paper, I have studied the forward production heavy quarks in the hybrid formalism in pA collisions. I provided the results for the single inclusive cross section for extrinsic charm and beauty hadron production at LO. Moreover, I have also studied their heavy quark limit and provided the expression up to order $1/m_Q^4$ and shown that in the heavy quark limit the production cross section is linearly proportional to square of the saturation momentum of the target.

Finally, in [P7], I have studied the extension of the "glasma graph approach" to the two gluon production from pp to pA collisions by including the multiple scattering effects of the dense target. The main difference between the work performed in [H9] and [P7] is the computation framework. The two gluon correlations in [P7] are calculated within the k_t-factorized approach which is difficult to generalize to three or more particles. Moreover, the results of [P7] are valid only valid in the large N_c limit as opposed to the the results of [H9] which is valid for finite N_c. In this sense, [P7] can be considered as the first attempt to generalize the "glasma graph approach" to the two gluon production from pp to pA collisions.

References

[1] V. N. Gribov, “A Reggeon Diagram Technique,” Sov. Phys. JETP **26**, 414 (1968) [Zh. Eksp. Teor. Fiz. **53**, 654 (1967)].

[2] V. N. Gribov and L. N. Lipatov, “Deep inelastic e p scattering in perturbation theory,” Sov. J. Nucl. Phys. **15**, 438 (1972) [Yad. Fiz. **15**, 781 (1972)].

[3] G. Altarelli and G. Parisi, “Asymptotic Freedom in Parton Language,” Nucl. Phys. B **126**, 298 (1977). doi:10.1016/0550-3213(77)90384-4

[4] Y. L. Dokshitzer, “Calculation of the Structure Functions for Deep Inelastic Scattering and e+ e- Annihilation by Perturbation Theory in Quantum Chromodynamics.,” Sov. Phys. JETP **46**, 641 (1977) [Zh. Eksp. Teor. Fiz. **73**, 1216 (1977)].

[5] E. A. Kuraev, L. N. Lipatov and V. S. Fadin, Sov. Phys. JETP **45**, 199 (1977) [Zh. Eksp. Teor. Fiz. **72**, 377 (1977)].

[6] I. I. Balitsky and L. N. Lipatov, "The Pomeranchuk Singularity in Quantum Chromodynamics," Sov. J. Nucl. Phys. **28**, 822 (1978) [Yad. Fiz. **28**, 1597 (1978)].

[7] M. Froissart, "Asymptotic behavior and subtractions in the Mandelstam representation," Phys. Rev. **123**, 1053 (1961). doi:10.1103/PhysRev.123.1053

[8] F. D. Aaron *et al.* [H1 and ZEUS Collaborations], "Combined Measurement and QCD Analysis of the Inclusive e+- p Scattering Cross Sections at HERA," JHEP **1001**, 109 (2010) doi:10.1007/JHEP01(2010)109 [arXiv:0911.0884 [hep-ex]].

[9] L. V. Gribov, E. M. Levin and M. G. Ryskin, "Semihard Processes in QCD," Phys. Rept. **100**, 1 (1983). doi:10.1016/0370-1573(83)90022-4

[10] A. H. Mueller, "Small x Behavior and Parton Saturation: A QCD Model," Nucl. Phys. B **335**, 115 (1990). doi:10.1016/0550-3213(90)90173-B

[11] A. H. Mueller, "Unitarity and the BFKL pomeron," Nucl. Phys. B **437**, 107 (1995) doi:10.1016/0550-3213(94)00480-3 [hep-ph/9408245].

[12] A. H. Mueller, "Soft gluons in the infinite momentum wave function and the BFKL pomeron," Nucl. Phys. B **415**, 373 (1994). doi:10.1016/0550-3213(94)90116-3

[13] A. H. Mueller and B. Patel, "Single and double BFKL pomeron exchange and a dipole picture of high-energy hard processes," Nucl. Phys. B **425**, 471 (1994) doi:10.1016/0550-3213(94)90284-4 [hep-ph/9403256].

[14] L. D. McLerran and R. Venugopalan, "Computing quark and gluon distribution functions for very large nuclei," Phys. Rev. D **49**, 2233 (1994) doi:10.1103/PhysRevD.49.2233 [hep-ph/9309289].

[15] L. D. McLerran and R. Venugopalan, "Gluon distribution functions for very large nuclei at small transverse momentum," Phys. Rev. D **49**, 3352 (1994) doi:10.1103/PhysRevD.49.3352 [hep-ph/9311205].

[16] A. Ayala, J. Jalilian-Marian, L. D. McLerran and R. Venugopalan, "Quantum corrections to the Weizsacker-Williams gluon distribution function at small x," Phys. Rev. D **53**, 458 (1996) doi:10.1103/PhysRevD.53.458 [hep-ph/9508302].

[17] J. Jalilian-Marian, A. Kovner, A. Leonidov and H. Weigert, "The BFKL equation from the Wilson renormalization group," Nucl. Phys. B **504**, 415 (1997) doi:10.1016/S0550-3213(97)00440-9 [hep-ph/9701284].

[18] J. Jalilian-Marian, A. Kovner, A. Leonidov and H. Weigert, "The Wilson renormalization group for low x physics: Towards the high density regime," Phys. Rev. D **59**, 014014 (1998) doi:10.1103/PhysRevD.59.014014 [hep-ph/9706377].

[19] J. Jalilian-Marian, A. Kovner and H. Weigert, "The Wilson renormalization group for low x physics: Gluon evolution at finite parton density," Phys. Rev. D **59**, 014015 (1998) doi:10.1103/PhysRevD.59.014015 [hep-ph/9709432].

[20] A. Kovner and J. G. Milhano, "Vector potential versus color charge density in low x evolution," Phys. Rev. D **61**, 014012 (2000) doi:10.1103/PhysRevD.61.014012 [hep-ph/9904420].

[21] A. Kovner, J. G. Milhano and H. Weigert, "Relating different approaches to nonlinear QCD evolution at finite gluon density," Phys. Rev. D **62**, 114005 (2000) doi:10.1103/PhysRevD.62.114005 [hep-ph/0004014].

[22] H. Weigert, "Unitarity at small Bjorken x," Nucl. Phys. A **703**, 823 (2002) doi:10.1016/S0375-9474(01)01668-2 [hep-ph/0004044].

[23] E. Iancu, A. Leonidov and L. D. McLerran, "Nonlinear gluon evolution in the color glass condensate. 1.," Nucl. Phys. A **692**, 583 (2001) doi:10.1016/S0375-9474(01)00642-X [hep-ph/0011241].

[24] E. Ferreiro, E. Iancu, A. Leonidov and L. McLerran, "Nonlinear gluon evolution in the color glass condensate. 2.," Nucl. Phys. A **703**, 489 (2002) doi:10.1016/S0375-9474(01)01329-X [hep-ph/0109115].

[25] I. Balitsky, "Operator expansion for high-energy scattering," Nucl. Phys. B **463**, 99 (1996) doi:10.1016/0550-3213(95)00638-9 [hep-ph/9509348].

[26] I. Balitsky, Phys. Rev. D **60**, 014020 (1999) doi:10.1103/PhysRevD.60.014020 [hep-ph/9812311].

[27] Y. V. Kovchegov, "Unitarization of the BFKL pomeron on a nucleus," Phys. Rev. D **61**, 074018 (2000) doi:10.1103/PhysRevD.61.074018 [hep-ph/9905214].

[28] Y. V. Kovchegov, "Small x F(2) structure function of a nucleus including multiple pomeron exchanges," Phys. Rev. D **60**, 034008 (1999) doi:10.1103/PhysRevD.60.034008 [hep-ph/9901281].

[29] Y. V. Kovchegov and K. Tuchin, "Inclusive gluon production in DIS at high parton density," Phys. Rev. D **65**, 074026 (2002) doi:10.1103/PhysRevD.65.074026 [hep-ph/0111362].

[30] A. Dumitru, A. Hayashigaki and J. Jalilian-Marian, "The Color glass condensate and hadron production in the forward region," Nucl. Phys. A **765**, 464 (2006) doi:10.1016/j.nuclphysa.2005.11.014 [hep-ph/0506308].

[31] Y. Mehtar-Tani, "Relating the description of gluon production in pA collisions and parton energy loss in AA collisions," Phys. Rev. C **75**, 034908 (2007) doi:10.1103/PhysRevC.75.034908 [hep-ph/0606236].

[32] T. Altinoluk and A. Kovner, "Particle Production at High Energy and Large Transverse Momentum - 'The Hybrid Formalism' Revisited," Phys. Rev. D **83**, 105004 (2011) doi:10.1103/PhysRevD.83.105004 [arXiv:1102.5327 [hep-ph]].

[33] G. A. Chirilli, B. W. Xiao and F. Yuan, "One-loop Factorization for Inclusive Hadron Production in pA Collisions in the Saturation Formalism," Phys. Rev. Lett. **108**, 122301 (2012) doi:10.1103/PhysRevLett.108.122301 [arXiv:1112.1061 [hep-ph]].

[34] G. A. Chirilli, B. W. Xiao and F. Yuan, "Inclusive Hadron Productions in pA Collisions," Phys. Rev. D **86**, 054005 (2012) doi:10.1103/PhysRevD.86.054005 [arXiv:1203.6139 [hep-ph]].

[35] Z. B. Kang, I. Vitev and H. Xing, "Next-to-leading order forward hadron production in the small-x regime: rapidity factorization," Phys. Rev. Lett. **113**, 062002 (2014) doi:10.1103/PhysRevLett.113.062002 [arXiv:1403.5221 [hep-ph]].

[36] A. M. Stasto, B. W. Xiao and D. Zaslavsky, "Towards the Test of Saturation Physics Beyond Leading Logarithm," Phys. Rev. Lett. **112**, no. 1, 012302 (2014) doi:10.1103/PhysRevLett.112.012302 [arXiv:1307.4057 [hep-ph]].

[37] I. Arsene *et al.* [BRAHMS Collaboration], "On the evolution of the nuclear modification factors with rapidity and centrality in d + Au collisions at s(NN)**(1/2) = 200-GeV," Phys. Rev. Lett. **93**, 242303 (2004) doi:10.1103/PhysRevLett.93.242303 [nucl-ex/0403005].

[38] K. Watanabe, B. W. Xiao, F. Yuan and D. Zaslavsky, "Implementing the exact kinematical constraint in the saturation formalism," Phys. Rev. D **92**, no. 3, 034026 (2015) doi:10.1103/PhysRevD.92.034026 [arXiv:1505.05183 [hep-ph]].

[39] F. Dominguez, C. Marquet, B. W. Xiao and F. Yuan, "Universality of Unintegrated Gluon Distributions at small x," Phys. Rev. D **83**, 105005 (2011) doi:10.1103/PhysRevD.83.105005 [arXiv:1101.0715 [hep-ph]].

[40] A. van Hameren, P. Kotko, K. Kutak, C. Marquet and S. Sapeta, "Saturation effects in forward-forward dijet production in p+Pb collisions," Phys. Rev. D **89**, no. 9, 094014 (2014) doi:10.1103/PhysRevD.89.094014 [arXiv:1402.5065 [hep-ph]].

[41] P. Kotko, K. Kutak, C. Marquet, E. Petreska, S. Sapeta and A. van Hameren, "Improved TMD factorization for forward dijet production in dilute-dense hadronic collisions," JHEP **1509**, 106 (2015) doi:10.1007/JHEP09(2015)106 [arXiv:1503.03421 [hep-ph]].

[42] C. Marquet, E. Petreska and C. Roiesnel, "Transverse-momentum-dependent gluon distributions from JIMWLK evolution," JHEP **1610**, 065 (2016) doi:10.1007/JHEP10(2016)065 [arXiv:1608.02577 [hep-ph]].

[43] C. Marquet, C. Roiesnel and P. Taels, "Linearly polarized small-x gluons in forward heavy-quark pair production," Phys. Rev. D **97**, no. 1, 014004 (2018) doi:10.1103/PhysRevD.97.014004 [arXiv:1710.05698 [hep-ph]].

[44] V. Khachatryan *et al.* [CMS Collaboration], "Observation of Long-Range Near-Side Angular Correlations in Proton-Proton Collisions at the LHC," JHEP **1009**, 091 (2010) doi:10.1007/JHEP09(2010)091 [arXiv:1009.4122 [hep-ex]].

[45] V. Khachatryan *et al.* [CMS Collaboration], "Measurement of long-range near-side two-particle angular correlations in pp collisions at $\sqrt{s}$ =13 TeV," Phys. Rev. Lett. **116** (2016) no.17, 172302 doi:10.1103/PhysRevLett.116.172302 [arXiv:1510.03068 [nucl-ex]].

[46] G. Aad *et al.* [ATLAS Collaboration], "Observation of Long-Range Elliptic Azimuthal Anisotropies in $\sqrt{s}$ =13 and 2.76 TeV *pp* Collisions with the ATLAS Detector," Phys. Rev. Lett. **116**, no. 17, 172301 (2016) doi:10.1103/PhysRevLett.116.172301 [arXiv:1509.04776 [hep-ex]].

[47] S. Chatrchyan *et al.* [CMS Collaboration], "Observation of long-range near-side angular correlations in proton-lead collisions at the LHC," Phys. Lett. B **718**, 795 (2013) doi:10.1016/j.physletb.2012.11.025 [arXiv:1210.5482 [nucl-ex]].

[48] B. Abelev *et al.* [ALICE Collaboration], "Long-range angular correlations on the near and away side in p-Pb collisions at $\sqrt{s_{NN}} = 5.02$ TeV," Phys. Lett. B **719**, 29 (2013) doi:10.1016/j.physletb.2013.01.012 [arXiv:1212.2001 [nucl-ex]].

[49] G. Aad *et al.* [ATLAS Collaboration], Phys. Rev. Lett. **110**, no. 18, 182302 (2013) doi:10.1103/PhysRevLett.110.182302 [arXiv:1212.5198 [hep-ex]].

[50] R. Aaij *et al.* [LHCb Collaboration], "Measurements of long-range near-side angular correlations in $\sqrt{s_{\rm NN}} = 5$TeV proton-lead collisions in the forward region," Phys. Lett. B **762**, 473 (2016) doi:10.1016/j.physletb.2016.09.064 [arXiv:1512.00439 [nucl-ex]].

[51] B. Alver *et al.* [PHOBOS Collaboration], "System size dependence of cluster properties from two-particle angular correlations in Cu+Cu and Au+Au collisions at s(NN)**(1/2) = 200-GeV," Phys. Rev. C **81**, 024904 (2010) doi:10.1103/PhysRevC.81.024904 [arXiv:0812.1172 [nucl-ex]].

[52] B. Alver *et al.* [PHOBOS Collaboration], "High transverse momentum triggered correlations over a large pseudorapidity acceptance in Au+Au collisions at s(NN)**1/2 = 200 GeV," Phys. Rev. Lett. **104**, 062301 (2010) doi:10.1103/PhysRevLett.104.062301 [arXiv:0903.2811 [nucl-ex]].

[53] B. I. Abelev *et al.* [STAR Collaboration], Phys. Rev. Lett. **105**, 022301 (2010) doi:10.1103/PhysRevLett.105.022301 [arXiv:0912.3977 [hep-ex]].

[54] A. Dumitru, F. Gelis, L. McLerran and R. Venugopalan, "Glasma flux tubes and the near side ridge phenomenon at RHIC," Nucl. Phys. A **810**, 91 (2008) doi:10.1016/j.nuclphysa.2008.06.012 [arXiv:0804.3858 [hep-ph]].

[55] K. Dusling, F. Gelis, T. Lappi and R. Venugopalan, "Long range two-particle rapidity correlations in A+A collisions from high energy QCD evolution," Nucl. Phys. A **836**, 159 (2010) doi:10.1016/j.nuclphysa.2009.12.044 [arXiv:0911.2720 [hep-ph]].

[56] A. Dumitru, K. Dusling, F. Gelis, J. Jalilian-Marian, T. Lappi and R. Venugopalan, "The Ridge in proton-proton collisions at the LHC," Phys. Lett. B **697**, 21 (2011) doi:10.1016/j.physletb.2011.01.024 [arXiv:1009.5295 [hep-ph]].

[57] K. Dusling and R. Venugopalan, "Azimuthal collimation of long range rapidity correlations by strong color fields in high multiplicity hadron-hadron collisions," Phys. Rev. Lett. **108**, 262001 (2012) doi:10.1103/PhysRevLett.108.262001 [arXiv:1201.2658 [hep-ph]].

[58] K. Dusling and R. Venugopalan, "Evidence for BFKL and saturation dynamics from dihadron spectra at the LHC," Phys. Rev. D **87**, no. 5, 051502 (2013) doi:10.1103/PhysRevD.87.051502 [arXiv:1210.3890 [hep-ph]].

[59] K. Dusling and R. Venugopalan, "Explanation of systematics of CMS p+Pb high multiplicity di-hadron data at $\sqrt{s}_{\rm NN} = 5.02$ TeV," Phys. Rev. D **87**, no. 5, 054014 (2013) doi:10.1103/PhysRevD.87.054014 [arXiv:1211.3701 [hep-ph]].

[60] K. Dusling and R. Venugopalan, "Comparison of the color glass condensate to dihadron correlations in proton-proton and proton-nucleus collisions," Phys. Rev. D **87**, no. 9, 094034 (2013) doi:10.1103/PhysRevD.87.094034 [arXiv:1302.7018 [hep-ph]].

[61] K. Dusling, M. Mace and R. Venugopalan, "Multiparticle collectivity from initial state correlations in high energy proton-nucleus collisions," Phys. Rev. Lett. **120**, no. 4, 042002 (2018) doi:10.1103/PhysRevLett.120.042002 [arXiv:1705.00745 [hep-ph]].

[62] K. Dusling, M. Mace and R. Venugopalan, "Parton model description of multiparticle azimuthal correlations in pA collisions," Phys. Rev. D **97**, no. 1, 016014 (2018) doi:10.1103/PhysRevD.97.016014 [arXiv:1706.06260 [hep-ph]].

[63] I. Balitsky and A. Tarasov, "Rapidity evolution of gluon TMD from low to moderate x," JHEP **1510**, 017 (2015) doi:10.1007/JHEP10(2015)017 [arXiv:1505.02151 [hep-ph]].

[64] I. Balitsky and A. Tarasov, "Gluon TMD in particle production from low to moderate x," JHEP **1606**, 164 (2016) doi:10.1007/JHEP06(2016)164 [arXiv:1603.06548 [hep-ph]].

[65] Y. V. Kovchegov, D. Pitonyak and M. D. Sievert, "Helicity Evolution at Small-x," JHEP **1601**, 072 (2016) Erratum: [JHEP **1610**, 148 (2016)] doi:10.1007/JHEP01(2016)072, 10.1007/JHEP10(2016)148 [arXiv:1511.06737 [hep-ph]].

[66] Y. V. Kovchegov, D. Pitonyak and M. D. Sievert, "Helicity Evolution at Small x: Flavor Singlet and Non-Singlet Observables," Phys. Rev. D **95**, no. 1, 014033 (2017) doi:10.1103/PhysRevD.95.014033 [arXiv:1610.06197 [hep-ph]].

[67] G. A. Chirilli, "Sub-eikonal corrections to scattering amplitudes at high energy," JHEP **1901**, 118 (2019) doi:10.1007/JHEP01(2019)118 [arXiv:1807.11435 [hep-ph]].

[68] E. Iancu, A. H. Mueller and D. N. Triantafyllopoulos, JHEP **1612**, 041 (2016) doi:10.1007/JHEP12(2016)041 [arXiv:1608.05293 [hep-ph]].

[69] T. Lappi, B. Schenke, S. Schlichting and R. Venugopalan, "Tracing the origin of azimuthal gluon correlations in the color glass condensate," JHEP **1601**, 061 (2016) doi:10.1007/JHEP01(2016)061 [arXiv:1509.03499 [hep-ph]].

[70] M. Mace, V. V. Skokov, P. Tribedy and R. Venugopalan, "Hierarchy of azimuthal anisotropy harmonics in collisions of small systems from the Color Glass Condensate," Phys. Rev. Lett. **121**, no. 5, 052301 (2018) doi:10.1103/PhysRevLett.121.052301 [arXiv:1805.09342 [hep-ph]].

[71] M. Mace, V. V. Skokov, P. Tribedy and R. Venugopalan, "Initial state description of azimuthally collimated long range correlations in ultrarelativistic light-heavy ion collisions," arXiv:1901.10506 [hep-ph].

[72] A. Kovner, M. Lublinsky and V. Skokov, "Exploring correlations in the CGC wave function: odd azimuthal anisotropy," Phys. Rev. D **96**, no. 1, 016010 (2017) doi:10.1103/PhysRevD.96.016010 [arXiv:1612.07790 [hep-ph]].

[73] Y. V. Kovchegov and V. V. Skokov, "How classical gluon fields generate odd azimuthal harmonics for the two-gluon correlation function in high-energy collisions," Phys. Rev. D **97**, no. 9, 094021 (2018) doi:10.1103/PhysRevD.97.094021 [arXiv:1802.08166 [hep-ph]].

[74] M. Mace, V. V. Skokov, P. Tribedy and R. Venugopalan, "Systematics of azimuthal anisotropy harmonics in proton–nucleus collisions at the LHC from the Color Glass Condensate," Phys. Lett. B **788**, 161 (2019) doi:10.1016/j.physletb.2018.09.064 [arXiv:1807.00825 [hep-ph]].

[75] P. Agostini, T. Altinoluk and N. Armesto, "Non-eikonal corrections to multi-particle production in the Color Glass Condensate," arXiv:1902.04483 [hep-ph].

[76] T. Altinoluk, R. Boussarie, C. Marquet and P. Taels, "TMD factorization for dijets + photon production from the dilute-dense CGC framework," arXiv:1810.11273 [hep-ph].

[77] T. Altinoluk, R. Boussarie and P. Kotko, "Interplay of the CGC and TMD frameworks to all orders in kinematic twist," arXiv:1901.01175 [hep-ph].

[78] T. Altinoluk and R. Boussarie, "Low x physics as an infinite twist (G)TMD framework: unravelling the origins of saturation," arXiv:1902.07930 [hep-ph].

[79] T. Altinoluk, A. Kovner, M. Lublinsky and J. Peressutti, "QCD Reggeon Field Theory for every day: Pomeron loops included," JHEP **0903**, 109 (2009) doi:10.1088/1126-6708/2009/03/109 [arXiv:0901.2559 [hep-ph]].

[80] T. Altinoluk, A. Kovner and M. Lublinsky, "Inclusive Gluon Production in the QCD Reggeon Field Theory: Pomeron Loops Included," JHEP **0903**, 110 (2009) doi:10.1088/1126-6708/2009/03/110 [arXiv:0901.2560 [hep-ph]].

Tolga ALTINOLUK